Estimation of damping through internally excited roll tests

Adriana Oliva-Remola [a], Gabriele Bulian [b,*], Luis Pérez-Rojas [a]

[a] CEHINAV Research Group, ETSIN, Universidad Politécnica de Madrid, Avda. de la Memoria, 4, 28040 Madrid, Spain
[b] Department of Engineering and Architecture, University of Trieste, Via A. Valerio 10, 34127 Trieste, Italy

ARTICLE INFO

Keywords:
Roll damping
Internal excitation
Fishing vessels
Nonlinear rolling
Experimental techniques

ABSTRACT

Roll damping represents a key factor for a proper estimation of the ship behaviour in a seaway. However, due to the typical dominance of viscous effects, accurately estimating roll damping is a challenging task. The most common experimental approach for determining roll damping parameters is based on the analysis of roll decays, although forced and excited roll tests in calm water or in waves have been used as well. This paper proposes a technique for estimating roll damping from internally excited roll tests in calm water. Tests are performed by exciting roll motion through an internal shifting mass. Roll damping parameters can then be determined from the analysis of the obtained roll response curves. The paper describes the experimental technique and a nonlinear mathematical model for representing the system dynamics. A procedure is proposed for determining roll damping coefficients, using, as a basis for the analysis, the developed mathematical model. A case study is reported where damping coefficients are determined for a trawler fishing vessel using the proposed technique. Obtained results are compared with those from standard roll decays analysis. For model validation purposes, the experimental roll response curves are also compared with those simulated through the developed mathematical model.

1. Introduction

From a seakeeping perspective, ship roll damping represents a key factor for a proper estimation of the ship roll behaviour in a seaway. Moreover, from a regulatory, and hence design, perspective roll damping is a major parameter in some stability-related international regulations. This is the case of MSC.1/Circ.1200 (IMO, 2006), which addresses the alternative experimental assessment of the Weather Criterion, and where roll damping may be necessary to determine the regular waves roll-back angle when direct experimentation cannot be carried out. Damping is also fundamental in case of the majority of failure modes addressed by the, still under development, Second Generation Intact Stability Criteria (SGISC) (e.g. IMO, 2016, 2017; Peters et al., 2012). However, due to the typical dominance of viscous effects, accurately determining roll damping is a challenging task.

Roll damping was already considered by Froude (Froude et al., 1955) and, since his seminal contributions, this topic has continued gaining attention over the years. Research studies were and are still focused on different complementary aspects. Large attention has been given to the analytical mathematical modelling of roll damping and to the corresponding analysis of experimental data (e.g. Bulian, 2004; Cardo et al., 1982; Dalzell, 1978; Francescutto and Contento, 1999; Haddara and Bennett, 1989; Park et al., 2017; Roberts, 1985; Spyrou and Thompson, 2000). Nonlinear roll damping prediction at design stage has mostly been based on semi-empirical methods (see, e.g. Himeno, 1981; ITTC, 2011; Ikeda et al., 1978; Kawahara et al., 2012; and see references in the review regarding semi-empirical methods by Falzarano et al., 2015) and on the use of experimental reference data sets (e.g. Blume, 1979). Recently, thanks to the increase of available computational resources and thanks to the improvement of numerical methods, also CFD simulations have started being applied for the estimation of roll damping (see, e.g. Handschel et al., 2012; Hua et al., 2011; Irkal et al., 2016; Ommani et al., 2015; as well as references in the literature review by Bačkalov et al., 2016). While the effort on roll damping modelling and estimation was originally placed into small and medium ship roll angles, more focus is presently given to large angles of roll (Bačkalov et al., 2016). The need to have a proper estimation of roll damping at large rolling amplitudes is linked more to safety rather than to operability. It is therefore understandable that large amplitude roll damping may represent a relevant topic from a regulatory perspective when ship roll motion is directly addressed (IMO, 2006, 2016, 2017; Peters et al., 2012). Current semi-empirical methods, such as the (Simplified) Ikeda's Method (Kawahara et al., 2012), are limited to cargo vessels and specific ranges of hull particulars (Falzarano et al., 2015), although some attempts have

* Corresponding author.
E-mail addresses: adriana.oliva@upm.es (A. Oliva-Remola), gbulian@units.it (G. Bulian), luis.perezrojas@upm.es (L. Pérez-Rojas).

Accepted 15 April 2018

been made to apply semi-empirical methods to other types of ships such as fishing vessels (Aarsæther et al., 2015; Ali et al., 2004; Kuroda et al., 2003; Míguez González et al., 2013; Paroka and Umeda, 2007). However, such semi-empirical methods have been criticised for lacking accuracy at large roll angles (Bassler, 2013). Hence, as stated in the draft guidelines for direct stability assessment procedures in the framework of SGISC (IMO, 2017), the preferred source of the data to be used for the calibration of roll damping in motion prediction codes should be experimental roll decays or excited roll tests.

In the past, studies have been dedicated to the different experimental procedures which can be followed to gather data for the determination of roll damping. The most typical means for roll damping determination is based on the execution and processing of roll decays. However, excited roll tests may offer advantages with respect to roll decays. In fact, one typical problem associated with roll damping estimation based on roll decays is the difficulty in gathering damping information at large rolling angles. Instead, excited roll tests can allow achieving large rolling oscillation angles by properly modifying the forcing. Different types of roll tests in calm water can be carried out for roll damping estimation, either with free model (excited tests) or with fixed axis (forced tests) (e.g. Blume, 1979; Bertaglia et al., 2004; Handschel and Abdel-Maksoud, 2014; Handschel et al., 2015; Spouge et al., 1986; Wassermann et al., 2016). Moreover, experimental tests in regular beam waves can also be used to identify roll damping through parameter identification techniques (e.g. Bertaglia et al., 2004; Contento et al., 1996; Francescutto and Contento, 1998, 1999; Francescutto et al., 1998; IMO, 2006).

Despite experimental tests are the most accepted way to reliably estimate ship roll damping, different alternative approaches still coexist in available international guidelines (e.g. ITTC, 2011; IMO, 2006). Since different experimental approaches are associated with different hydrodynamic scenarios, estimated roll damping may, in principle, differ depending on the used approach. These possible differences have often been neglected, although some studies focusing on this aspect appear to be available in literature (e.g. Bertaglia et al., 2004; Handschel and Abdel-Maksoud, 2014; Handschel et al., 2015; Mathisen and Price, 1985; Wassermann et al., 2016).

Considering the reported background, the scope of the present paper is two-fold. Firstly, the paper presents a methodology to perform and analyse excited roll experiments in calm water, based on the generation of roll excitation through an internally moving mass. Secondly, the paper presents comparisons between roll damping estimated from the proposed excited roll tests and from standard roll decays. The experimental setup used herein for the excitation of roll motion is similar to that used by Bulian et al. (2010) to excite the rotational motion of a free surface tank having a fixed axis. The main advantages of the proposed tests are the full knowledge of the excitation from first-principle mechanics considerations, and the possibility of exciting the model up to large rolling angles.

The paper is organised as follows. Firstly, the proposed methodology is presented. The description of the methodology comprises the description of the experimental setup, the derivation of a 1-DOF mathematical model of roll motion to be used for roll damping assessment, and the description of a procedure for the determination of roll damping coefficients from experimental results. Secondly, a case study is reported. Experimental tests are carried out for a trawler fishing vessel according to the proposed technique. The hull is described, together with the tested loading conditions. Results from excited roll tests are reported, and then corresponding data are analysed to obtain roll damping coefficients according to the proposed procedure. A validation of the mathematical model, using fitted roll damping coefficients, is also reported, both in terms of roll response curves as well as in terms of roll time histories. The case study concludes with a comparison between roll damping estimated in accordance with the proposed procedure, and roll damping estimated from the analysis of roll decays. Details of the roll decays analysis procedure are described in a separate Appendix. Eventually, some concluding remarks are provided.

2. Methodology

This section presents the methodology for the determination of roll damping parameters. The experimental setup is firstly described. Afterwards, the mathematical modelling used for describing the system dynamics is presented. Finally, a methodology for the determination of roll damping coefficients from the obtained experimental data, using the developed mathematical model, is proposed.

2.1. Experimental setup

In the proposed technique, the ship model is freely floating (or at most softly restrained) in calm water and it is excited to roll using an internal shifting mass that moves following a prescribed movement. This type of technique has been referred to in the past as "harmonic excited roll motion (HERM)" technique (Handschel and Abdel-Maksoud, 2014; Handschel et al., 2015; Wassermann et al., 2016). Internally excited roll motion tests have the benefit of potentially allowing the determination of roll damping also at large rolling amplitudes, which are the amplitude ranges typically relevant for ship safety assessment. Obtaining roll damping at large rolling angles through roll decays is, instead, typically difficult (or even impossible), due to the strong natural reduction of roll amplitude in the first oscillation cycles and due to the difficulties associated with the inclining of models at too large initial angles if models are large. Moreover, internally excited roll tests without hard constraints on the model have the benefit of maintaining the natural coupling between roll motion and other relevant motions (particularly sway). This characteristic, instead, is lost when forced tests are carried out with fixed axis, and the correspondingly determined roll damping is therefore affected (see Bačkalov et al., 2016).

The mass in the present experimental techniques moves along a linear guide, and the prescribed motion of the mass, which then generates the internal excitation, is sinusoidal. The guide is fixed to the ship model near its centre of gravity and the movement of the mass is obtained through a controllable electrical engine connected to an encoder, as shown in Fig. 1. The maximum amplitude of the moving mass is directly limited by the overall dimensions of the linear guide. For the case study reported hereinafter, the length of the guide corresponds to 206 *mm*. The moving mass is initially placed at the centre of the guide and it is allowed to move from the centre up to 90 *mm* on each side, which therefore corresponds to the maximum amplitude of transversal motion of the mass ($y_{m,max}$). The oscillation frequency of the moving mass can be varied from 0.1 *rad/s* to 7.0 *rad/s*, corresponding to a range of forcing periods from 0.9 *s* to 62.8 *s*.

Different forcing cases (*FC*) can be generated by different combinations of the moving mass (m_m) and maximum motion amplitude. However, in the present tests, only the moving mass has been changed, keeping always the same maximum amplitude of motion ($y_{m,max} = 90\ mm$). Each forcing case can be associated with a nominal amplitude of forcing (A_{FC}), which is defined as follows:

$$A_{FC} = m_m g y_{m,max} \tag{1}$$

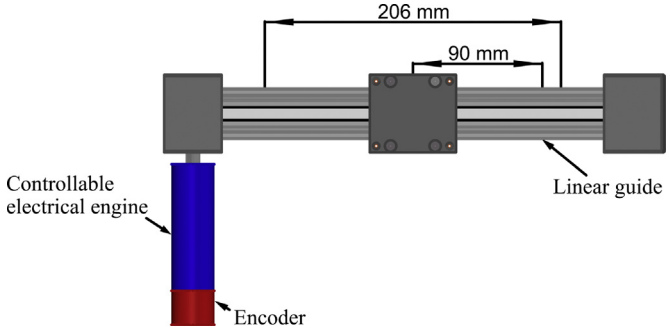

Fig. 1. Details of the linear guide.

In addition, it is also useful to associate to each forcing case the static heel (α_{FC}) that the ship model reaches when the moving mass is placed at the extreme position $y_{m,max}$. Translations and rotations of the vessel during the tests are measured using the commercial optical motion capture system "Optitrack Flex 3" (Optitrack, 2017), whereas the actual internal mass motion is recorded from the encoder signal (mainly for checking purposes).

The positioning of the linear guide on the ship model used for the present case study is shown in Fig. 2 and Fig. 3. Fig. 3 also shows the positioning of the trackable markers of the optical system. In addition, Fig. 3 reports the shifting mass, and associated guide, which, as described hereinafter in the section reporting the case study, was used to experimentally determine the ship roll restoring moment for verification purposes.

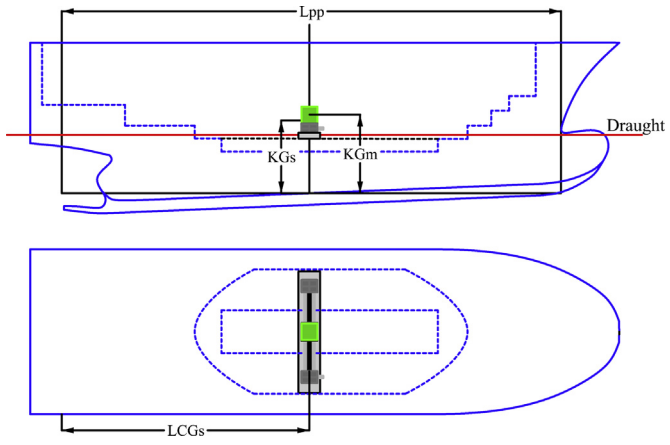

Fig. 2. Positioning of the linear guide.

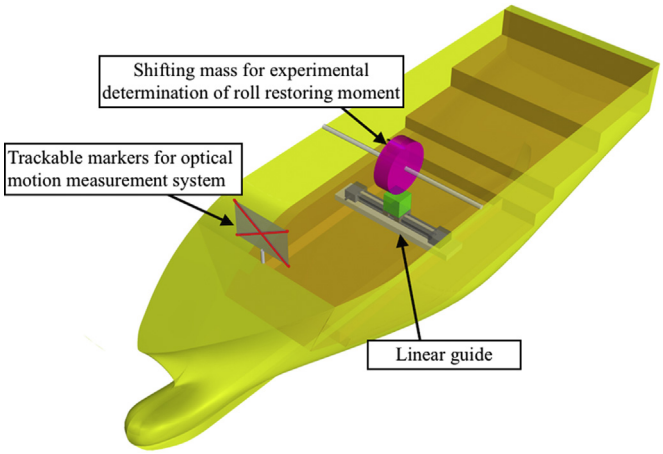

Fig. 3. Perspective view of the experimental setup.

2.2. Mathematical model

Scope of the tests where roll is excited by the internal moving mass, is to provide a set of data from which roll damping coefficients can be determined, with particular attention to cover a large range of rolling amplitudes (which is something typically difficult through roll decays). To this end, it is necessary to have at disposal a mathematical model of roll dynamics under such conditions. Scope of the mathematical model is to describe the dynamics of the system in a general form, taking into account the actual excitation provided by the moving mass. In fact, the internally moving mass generates forces and moments on the vessel which, in principle, cannot be simplified as a quasi-static weight shift. It is therefore important that the excitation from the mass is properly modelled through first-principles mechanics. Moreover, the mathematical model shall embed damping in a parametric form suitable for parameters identification using available experimental data. Finally, it is necessary that the mathematical model maintains a proper balance between simplicity and accuracy, in order for it to be practical in potentially routine applications.

Therefore, this section reports the development of a simplified mathematical model for describing the system dynamics under excited roll tests with internally moving mass. First, the dynamics of the system is described through 6-DOF nonlinear equations. Then, the equations of motion are reduced by simplifying the system to a 2-DOF nonlinear system accounting only for roll and sway motions. Finally, the 2-DOF equations are algebraically manipulated and some further assumptions are introduced in order to arrive at a 1-DOF roll motion equation, which will represent the basis for the damping identification technique.

In the development of the modelling, two right-handed reference systems will be considered: an earth fixed reference system (e.f.r.s.) ΩXYZ, and a body fixed reference system (b.f.r.s.) $Oxyz$. First and second derivatives as determined in the e.f.r.s. are indicated as single and double overdots, respectively, whereas the first and second derivatives in the b.f.r.s. are indicated as single and double prime, respectively.

2.2.1. 6-DOF equations of motion

The starting point for the development of the mathematical model are the general 6-DOF equations of motion of the ship. Herein, equations are written with reference to the coordinates of the origin O of the ship fixed reference system expressed in the earth fixed reference system, and in terms of angular momentum vector. The moving mass m_m is modelled as a point mass with prescribed motion in the b.f.r.s.

Equations of motion can therefore be written as follows:

$$
\begin{cases}
(m_s+m_m)\ddot{\underline{X}}_O+\underset{S\to\Sigma}{\ddot{\underline{R}}}\left(m_s\underline{\delta}_{G_S}+m_m\underline{\delta}_m(t)\right)+ \\
+2m_m\underset{S\to\Sigma}{\dot{\underline{R}}}\,\underline{\delta}_m{}'(t)+m_m\underset{S\to\Sigma}{\underline{R}}\,\underline{\delta}_m{}''(t)=\underline{F}_s^{ext}+\underline{F}_m^{ext} \\
\dfrac{d}{dt}\underline{L}_{G_s,s}+\left(\underset{S\to\Sigma}{\underline{R}}\left(m_s\underline{\delta}_{G_S}+m_m\underline{\delta}_m(t)\right)\right)\wedge\ddot{\underline{X}}_O+ \\
+\left(\underset{S\to\Sigma}{\underline{R}}\,\underline{\delta}_{G_S}\right)\wedge\left(\underset{S\to\Sigma}{\ddot{\underline{R}}}\left(m_s\underline{\delta}_{G_S}\right)\right)+\left(\underset{S\to\Sigma}{\underline{R}}\,\underline{\delta}_m(t)\right)\wedge\left(\underset{S\to\Sigma}{\ddot{\underline{R}}}\left(m_m\underline{\delta}_m(t)\right)\right)+ \\
+\left(\underset{S\to\Sigma}{\underline{R}}\,\underline{\delta}_m(t)\right)\wedge\left(2m_m\underset{S\to\Sigma}{\dot{\underline{R}}}\,\underline{\delta}_m{}'(t)+m_m\underset{S\to\Sigma}{\underline{R}}\,\underline{\delta}_m{}''(t)\right)= \\
=\underline{M}_{o,s}^{ext}+\left(\underset{S\to\Sigma}{\underline{R}}\,\underline{\delta}_m(t)\right)\wedge\underline{F}_m^{ext}
\end{cases}
\tag{2}
$$

In (2), one underlining indicates vectors while two underlining indicates matrices, and the symbol "$\wedge$" indicates the cross product. The quantities appearing in the equations are defined as follows, together with their units:

- m_m : [kg] mass of the moving mass (assumed to be a point mass);
- m_s : [kg] mass of the ship (without m_m);
- O : reference point, corresponding to the origin of the b.f.r.s.;
- G_s : centre of gravity of the ship (without m_m);
- $\underline{X}_O$: position vector of the point O expressed in the e.f.r.s;
- $\underset{S\to\Sigma}{\underline{\underline{R}}}$: transformation (rotation) matrix from b.f.r.s. to e.f.r.s.;
- $\underline{\delta}_{G_S}$: [m] relative position vector of point G_s with respect to O, expressed in the b.f.r.s.;
- $\underline{\delta}_m(t)$: [m] relative position vector of (centre of gravity of) the moving mass with respect to O, expressed in the b.f.r.s.;

- $\underline{L}_{G_s,s}$: $[kg{\cdot}m^2/s]$ angular momentum of the ship (without m_m) with respect to G_s, expressed in components with respect to the e.f.r.s.;
- $\underline{F}_s^{ext}$: $[N]$ vector of external forces acting on the ship (weight and fluid-structure interaction, plus other external forces, if present), expressed in components with respect to the e.f.r.s.;
- $\underline{M}_{o,s}^{ext}$: $[N{\cdot}m]$ moment of external forces acting on the ship (weight and fluid-structure interaction, plus others if present) calculated with respect to O, expressed in components with respect to the e.f.r.s.;
- $\underline{F}_m^{ext}$: $[N]$ vector of external forces acting on the moving mass (weight), expressed in components with respect to the e.f.r.s.;

It is herein noted that the reference point O used in the motion equations (2) is a generic ship-fixed reference point.

2.2.2. 2-DOF (roll and sway) equations of motion

The system of equations (2) is, in principle, appropriate for describing the global dynamics of the system. However, it is herein considered too complex for an effective use in the determination of roll damping parameters. Herein, therefore, a series of assumptions and simplifications are considered as follows, in order to transform the 6-DOF equations in a simplified 2-DOF model:

- The motion of the vessel is assumed to be (mainly) two-dimensional, and it is assumed that the dynamics can be described by considering only the sway translation of the point O plus a roll rotation ϕ. It is noted that the translation denoted herein as "sway" is a translation parallel to the calm water plane, i.e. a translation intended in the e.f.r.s. In addition, it is also noted that, as a consequence of this assumption, effects of coupling with yaw motion are neglected. Although this assumption is reasonable in case of zero speed tests (as in the case tests presented herein), its applicability in case of experiments with forward speed needs to be considered with care, and possibly checked.
- The point O is assumed to correspond to the intersection of the ship centreplane and the waterline of the vessel with zero heel and with the moving mass onboard.
- The vessel is assumed to be port/starboard symmetric and symmetrically loaded. As a result, the ship centre of gravity G_s is on the ship centreplane, i.e. $\underline{\delta}_{G_S} = (\delta_{G_S,x} \ , \ 0 \ , \ \delta_{G_S,z})^T$.
- The tensor of inertia of the ship (without the mass m_m) w.r.t. G_s is assumed to be (approximately) diagonal.
- The mass is assumed to translate only transversally in the b.f.r.s., which means that its position vector, in the b.f.r.s., can be expressed as $\underline{\delta}_m(t) = (\delta_{m,x} \ , \ y_m(t) \ , \ \delta_{m,z})^T$.
- For the rotated vessel, it is assumed that the buoyancy force vector ($\underline{\Delta}$), and the weight vector of the ship plus the mass ($\underline{W}_s + \underline{W}_m$) approximately compensate during the motion, i.e. $\underline{W}_s + \underline{W}_m + \underline{\Delta} \approx \underline{0}$.
- The force and the moment are split in two contributions:
  - One contribution due to the combination of weights (ship weight, moving mass) and buoyancy;
  - One contribution due to the fluid-structure interaction hydrodynamics.
- The hydrodynamic fluid-structure interaction force and moment are modelled using a combination of a linear hydrodynamic approach (for added mass terms) plus a nonlinear contribution. This latter contribution is assumed to comprise principally damping effects.
- The motion is assumed to be approximately harmonic, with a main forcing frequency ω $[rad/s]$, in such a way that constant frequency dependent added mass and damping terms can be considered for describing the fluid-structure interaction at steady state for each forcing condition.

According to the above assumptions, the original 6-DOF equations of motion (2) simplify as follows:

$$\begin{cases} (m_s+m_m)\ddot{Y}_O + [-(m_s+m_m)\cos(\phi)\delta_{Q,z} - m_m\sin(\phi)y_m(t)]\ddot{\phi} + \\ +[(m_s+m_m)\sin(\phi)\delta_{Q,z} - m_m\cos(\phi)y_m(t)]\dot{\phi}^2 + \\ -2m_m\sin(\phi)y_m'(t)\dot{\phi} + m_m\cos(\phi)y_m''(t) = \\ = -A_{22}(\omega)\ddot{Y}_O - A_{24}^O(\omega)\ddot{\phi} + F_{D,Y}(t) \\ \left[I_{G_s,s,xx} + m_s\delta_{G_s,z}^2 + m_m\left(\delta_{m,z}^2 + y_m^2(t)\right)\right]\ddot{\phi} + \\ +[-(m_s+m_m)\cos(\phi)\delta_{Q,z} - m_m\sin(\phi)y_m(t)]\ddot{Y}_O + \\ +2m_m y_m(t)y_m'(t)\dot{\phi} - m_m\delta_{m,z}y_m''(t) = \\ = -(m_s+m_m)g\overline{QZ}(\phi) - m_m g y_m(t)\cos(\phi) + \\ -A_{44}^O(\omega)\ddot{\phi} - A_{42}^O(\omega)\ddot{Y}_O + M_{O,D}(t) \end{cases} \tag{3}$$

where:

- Y_O : [m] is the horizontal lateral translation of point O in the e.f.r.s;
- ϕ : [rad] is the roll angle;
- Q : is the centre of mass of the ship when the mass m_m is on the centreplane. Accordingly, the coordinates of Q with respect to O in the b.f.r.s., can be determined as follows:

$$\begin{cases} \underline{\delta}_Q = \dfrac{(m_s\underline{\delta}_{G_S} + m_m\underline{\delta}_{m,xz})}{m_s+m_m} \\ \underline{\delta}_{m,xz} = (\delta_{m,x} \ , \ 0 \ , \ \delta_{m,z})^T \end{cases} \tag{4}$$

- $I_{G_s,s,xx}$: $[kg{\cdot}m^2]$ is the (dry) moment of inertia of the ship (without moving mass) w.r.t. a longitudinal axis x passing through G_s;
- y_m : $[m]$ is the instantaneous transversal coordinate of moving mass in the b.f.r.s.;
- $\overline{QZ}(\phi)$: $[m]$ is the hydrostatic roll righting lever w.r.t. point Q considering the vessel freely floating with displacement $\Delta = (m_s + m_m)g$. This term is meant to represent the hydrostatic contribution to the fluid-structure interaction force;
- $A_{22}(\omega)$: $[N/(m/s^2)]$ is the frequency dependent sway added mass;
- $A_{24}^O(\omega)$: $[N/(rad/s^2)]$ is the frequency dependent roll-to-sway added mass coefficient, w.r.t. point O;
- $A_{44}^O(\omega)$: $[N\cdot m/(rad/s^2)]$ is the frequency dependent roll added mass coefficient, w.r.t. point O;
- $A_{42}^O(\omega)$: $[N\cdot m/(m/s^2)]$ is the frequency dependent sway-to-roll added mass coefficient, w.r.t. point O;
- $F_{D,Y}(t)$: $[N]$ is the sway force associated with, possibly nonlinear, sway damping;
- $M_{O,D}(t)$: $[N\cdot m]$ is the roll moment w.r.t. point O associated with, possibly nonlinear, roll damping.

2.2.3. 1-DOF roll motion equation

The model (3) could in principle be used for modelling dissipation effects. This would require providing parametric models for the terms $F_{D,Y}(t)$ and $M_{O,D}(t)$, and it would require experimental measurement of both sway and roll. However, this is considered still too complex for the purpose of routine practical roll damping determination. Therefore, some additional simplifications are introduced in this section, with the intention of further reducing the model complexity. Scope of the simplifications introduced at this stage is, basically, to arrive at a 1-DOF equation of roll motion, which can be more directly used for roll damping identification purposes, starting from the availability of roll motion recordings from excited roll tests.

As a first step, the system of equations (3) is manipulated in such a way to obtain a single equation of roll motion. Basically, $\ddot{Y}_O$ is obtained from the first equation in (3) as a function of the remaining quantities, and it is then substituted in the second equation in (3). The following roll equation is then obtained:

$$
\begin{cases}
J_T(\phi,t)\ddot{\phi} = M_{\phi,hs}(\phi) + M^O_{\phi,RB}(t) + \\
\quad + M^O_{\phi,m_m}(\phi,t) - \dfrac{M_{42}(\phi,t) + A^O_{42}(\omega)}{M_{22} + A_{22}(\omega)} F_{Y,RB}(\phi,t) + M_{\phi,D}(\phi,t) \\
\text{with:} \\
J_T(\phi,t) = M_{44}(t) + A^O_{44}(\omega) - \dfrac{\left(M_{42}(\phi,t) + A^O_{42}(\omega)\right)\left(M_{24}(\phi,t) + A^O_{24}(\omega)\right)}{M_{22} + A_{22}(\omega)} \\
M_{44}(t) = I_{G_s,s,xx} + m_s \delta^2_{G_s,z} + m_m \left(\delta^2_{m,z} + y^2_m(t)\right) \\
M_{24}(\phi,t) = M_{42}(\phi,t) = -(m_s + m_m)\cos(\phi)\delta_{Q,z} - m_m \sin(\phi) y_m(t) \\
M_{22} = m_s + m_m \\
M_{\phi,hs}(\phi) = -(m_s + m_m) g \overline{QZ}(\phi) \\
M^O_{\phi,RB}(t) = -2 m_m y_m(t) y'_m(t) \\
M^O_{\phi,m_m}(\phi,t) = -m_m g y_m(t)\cos(\phi) + m_m \delta_{m,z} y''_m(t) - \dfrac{\left(M_{42}(\phi,t) + A^O_{42}(\omega)\right)}{M_{22} + A_{22}(\omega)} F_{Y,m_m}(t) \\
F_{Y,m_m}(\phi,t) = -m_m \cos(\phi) y''_m(t) \\
F_{Y,RB}(\phi,t) = -\left[(m_s + m_m)\sin(\phi)\delta_{Q,z} - m_m \cos(\phi) y_m(t)\right]\dot{\phi}^2 + 2 m_m \sin(\phi) y'_m(t)\dot{\phi} \\
M_{\phi,D}(\phi,t) = -\dfrac{\left(M_{42}(\phi,t) + A^O_{42}(\omega)\right)}{M_{22} + A_{22}(\omega)} F_{Y,D}(t) + M_{O,D}(t)
\end{cases}
\tag{5}
$$

The final simplification is to assume that the dissipative term $M_{\phi,D}(\phi,t)$ can be approximated as being explicitly dependent only on the roll velocity, as follows:

$$
M_{\phi,D}(\phi,t) \approx M_{\phi,D}\left(\dot{\phi}(t)\right) = -J_T(\phi,t) d\left(\dot{\phi}\right) \tag{6}
$$

It is also to be reminded that, according to (5), J_T is a frequency dependent term. Under the assumption (6), eq. (5) can be rewritten as follows:

$$
\begin{aligned}
&\ddot{\phi} + d\left(\dot{\phi}\right) + \frac{(m_s + m_m) g}{J_T(\phi,t)} \overline{QZ}(\phi) = \\
&= \frac{M^O_{\phi,RB}(t)}{J_T(\phi,t)} + \frac{M^O_{\phi,m_m}(\phi,t)}{J_T(\phi,t)} - \frac{M_{42}(\phi,t) + A^O_{42}(\omega)}{M_{22} + A_{22}(\omega)} \frac{F_{Y,RB}(\phi,t)}{J_T(\phi,t)}
\end{aligned}
\tag{7}
$$

Although different modelling can be used for the roll damping term $d(\dot{\phi})$, a typical expression, accounting for linear and nonlinear contributions, is as follows:

$$
d\left(\dot{\phi}\right) = 2\mu\dot{\phi} + \beta\dot{\phi}\left|\dot{\phi}\right| + \delta\dot{\phi}^3 \tag{8}
$$

where μ $[1/s]$, β $[1/rad]$ and δ $[s/rad^2]$ are, respectively, the linear, quadratic and cubic damping coefficients.

2.3. Procedure for the determination of damping coefficients

The model (7) can be used for the determination of roll damping parameters, starting from the availability of experimental roll response curves from excited roll tests. To this end, a Parameters Identification Technique (PIT) could be setup. Examples of PITs have been described by, e.g., Francescutto and Contento (1998, 1999), Francescutto et al. (1998), and in MSC.1/Circ.1200 (IMO, 2006).

The typical approach of PIT is, essentially, to define a set of free parameters in the mathematical model and then determine the optimum parameters by minimizing the error between predictions and measurements. Such an approach can, in principle, be applied using the mathematical model as a black-box.

In the present case, however, a slightly different approach is proposed. The approach is tailored to the specific problem at hand, it is considered to be informative for the user who has to carry out the determination of the roll damping coefficients, and it is deemed to be robust.

In the procedure described in the following, it is assumed that a series of forcing cases (FC) are considered. Each FC corresponds to a specific combination of moving mass and maximum mass displacement, and for each FC a roll response curve is obtained by carrying out experimental tests at different forcing frequencies. The resonance peak of the roll response curve, A_{res}, and the corresponding frequency, ω_{res}, are then obtained for each FC. Scope of the procedure is to fit roll damping coefficients in such a way that the mathematical model is able to reproduce approximately the same rolling amplitudes for the corresponding forcing cases. In the procedure described herein it is assumed that the mathematical model can capture, in a sufficiently accurate way, the peak resonance frequency ω_{res} for each FC. If the matching of the resonance frequencies is not sufficiently accurate, then a tuning of the dry inertia is assumed to be carried out through the inertia term $J_T(\phi,t)$. Added mass and inertia coefficients appearing in (7) are assumed to be pre-calculated for the considered ship draught and trim by means of numerical calculations (typically potential linear hydrodynamics). It is worth noting here that the methodology for the calculation of added mass and inertia coefficients (e.g. strip-theory or three-dimensional calculations) may affect the final result of the damping identification procedure. This aspect has not been addressed in this study, where, as described later, strip-theory calculations have been used for the determination of necessary hydrodynamic coefficients, and it would be worth to be further investigated.

The fitting of the experimental data is carried out in four main iterative steps, as follows:

- Step 1. For each FC a series of simulations of model (7) are carried out assuming a damping model characterised by an equivalent linear damping coefficient μ_{eq}, i.e.

$$
d\left(\dot{\phi}\right) = 2\mu_{eq}\dot{\phi} \tag{9}
$$

Different μ_{eq} coefficients are tested, in order to find the coefficient μ_{eq} which provides the same peak response amplitude as that obtained from the experiments for the considered forcing case. A first estimation of μ_{eq} is carried out by considering a simplified 1-DOF model, where the forcing from the moving mass is approximated by considering only the corresponding quasi-static heeling moment for small heeling angles, and for which an approximate peak rolling amplitude can be determined as follows:

$$
\begin{cases}
\ddot{\phi} + 2\mu_{eq}\dot{\phi} + \omega_0^2 \dfrac{\overline{QZ}(\phi)}{QM} = \omega_0^2 \dfrac{m_m g y_{m,max}}{\Delta QM} \sin(\omega t) \\
\text{At resonance: } 2\mu_{eq} A_{res} \omega_{res} \approx \omega_0^2 \dfrac{m_m g y_{m,max}}{\Delta QM} \Rightarrow \\
\qquad \Rightarrow \mu_{eq}(A_{res}, \omega_{res}) \approx \dfrac{\omega_0^2 m_m g y_{m,max}}{2 A_{res} \omega_{res} \Delta QM}
\end{cases}
\tag{10}
$$

where ω_0 $[rad/s]$ is the natural roll frequency, QM $[m]$ is the metacentric height w.r.t. point Q considering the vessel freely floating with displacement Δ ($QM = d\overline{QZ}/d\phi\big|_{\phi=0}$) and $y_{m,max}$ $[m]$ is the amplitude of mass translation. The final result in (10) comes from the fact that, at resonance, the inertial part and the restoring part of the equation of motion (approximately) cancel out, and therefore the amplitude of the damping term can be directly related to the amplitude of the forcing term at the peak response frequency. For a linear system there is a perfect cancelling between the inertial term and the restoring term when the forcing frequency is equal to the undamped roll natural frequency ω_0, and this frequency is very close to the peak response frequency when the system, as in case of roll, is very lightly damped. In case of nonlinear restoring the same concept can be applied with good approximation. In such case there is an approximate cancelling between the inertial part and the restoring part when

the system oscillates at its amplitude-dependent roll resonance frequency, i.e. when the response is along the system backbone curve.

It is also worth noting that the determination of μ_{eq} according to (10) can be considered as a small generalization of the Blume method (Blume, 1979; Handschel and Abdel-Maksoud, 2014). In fact, the Blume method assumes linear restoring, while μ_{eq} obtained according to (10) takes into account the possible shift of resonance frequency due to restoring nonlinearities, since, in general, it is $\omega_{res} \neq \omega_0$.

The equivalent linear damping coefficient μ_{eq} is then systematically varied around the first guess value obtained from (10), and the model (7) is simulated to obtain the peak amplitude and frequency of the roll response curve. The variation is specified in such a way that the range of peak amplitude values obtained from the simulations comprises the peak amplitude as obtained from the experiments. An example of graphical representation of results from this step is shown in Fig. 4, where different forcing cases (FC01 to FC07) are considered. It is noted that the figure shows the dependence between μ_{eq} and the product $A_{res}\omega_{res}$, because this representation will allow the same graph to be directly used for the determination of the nonlinear damping coefficients, as specified at the fourth step of the procedure.

- Step 2. Given the amplitude A_{res} and frequency ω_{res} of the experimental peaks for each FC, the actual equivalent linear damping coefficient value can be obtained, firstly, by interpolation as $\mu_{eq,interp}$, as shown in Fig. 5. Further simulations can be carried out in order to verify and, if necessary, refine, the value of μ_{eq} for each forcing case. However, considering the observed smooth behaviour of the dependence between μ_{eq} and A_{res} and ω_{res}, the interpolated value is expected to be sufficiently accurate. Eventually, from this step, the equivalent linear damping coefficient of the ship for the specific loading condition is obtained as a function of roll amplitude and a corresponding frequency. It is also noted that the determination of the equivalent linear damping is carried out through interpolation of μ_{eq} with respect to the rolling amplitude A_{res}, and not with respect to the product $A_{res}\omega_{res}$. Nevertheless, results are still reported as in Fig. 5 because this representation is more suitable for the final determination of nonlinear roll damping coefficients. It is however noted that, when the peak resonance frequencies are sufficiently well captured (see next step of the procedure), the interpolation based on A_{res} produces basically the same results as an interpolation based on $A_{res}\omega_{res}$.
- Step 3. This step is needed when peak frequencies of the roll response as obtained from simulations do not match the experimental peak frequencies. In such cases the dry radius of inertia of the vessel is tuned in order to better match the experimental results. Steps 1 and 2 are then repeated, following an iterative process until the peak amplitudes and frequencies from the simulations match the experimental ones. There are two main reasons requiring, typically, the tuning of the dry roll radius of inertia. One reason is associated with the fact that the dry roll radius of inertia may be unknown (as in the case presented herein) or it may be affected by measuring error which may be compensated by the tuning process. The second reason is associated with modelling aspects. In fact, the tuning of the dry roll radius of inertia can be considered as a practical way to compensate, to a certain extent, for the simplifications embedded in the simulation model (particularly regarding coupling among motions) and for the approximations/assumptions associated with the numerical estimation of hydrodynamic coefficients (added mass).

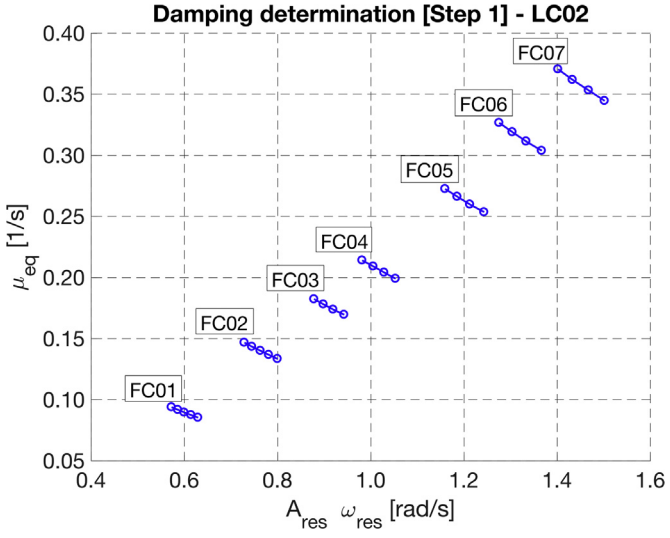

Fig. 4. Damping determination: Step 1.

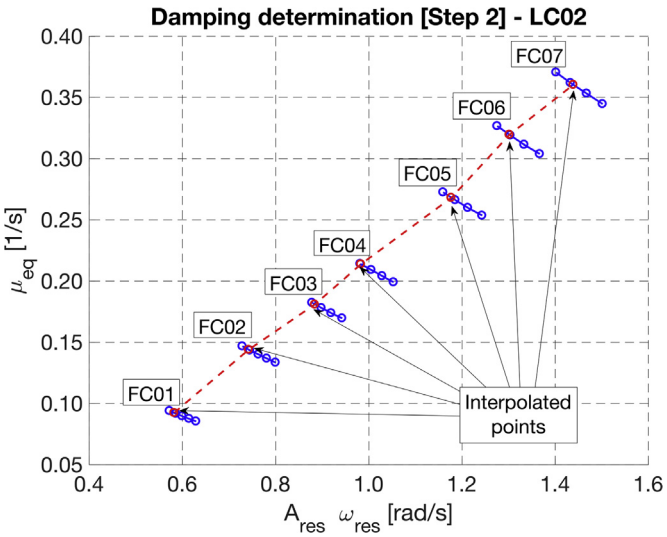

Fig. 5. Damping determination: Step 2.

- Step 4. The final step of the procedure is to use the obtained values of μ_{eq} for different combinations of amplitude and frequency, A_{res} and ω_{res}, in order to determine the characteristic coefficients for the nonlinear roll damping model. If the nonlinear roll damping model is assumed to be the typical model (8), linear and nonlinear damping coefficients can be determined from fitting, using the following relation (e.g. Bulian et al., 2009):

$$\mu_{eq}(A_{res},\omega_{res}) = \mu + \frac{4}{3\pi}\beta(A_{res}\omega_{res}) + \frac{3}{8}\delta(A_{res}\omega_{res})^2 \tag{11}$$

A similar approach can be used for any generic parameterised nonlinear roll damping model $d\left(\dot{\phi}|\underline{p}\right)$, where $\underline{p}$ is the set of parameters to be fitted, by requiring, in a least squares sense, that:

$$\begin{cases} \int_0^{2\pi/\omega_{res}} 2\mu_{eq}(A_{res},\omega_{res})\dot{\phi}^2 dt = \int_0^{2\pi/\omega_{res}} d\left(\dot{\phi}|\underline{p}\right)\dot{\phi}dt \\ \dot{\phi} = A_{res}\omega_{res}\sin(\omega_{res}t) \end{cases} \tag{12}$$

An example of fitting is shown in Fig. 6, where the quadratic damping coefficient in (11) was fixed to zero, and, therefore, the fitting was based on the a-priori assumption of a linear plus cubic roll damping model.

3. Case study

3.1. Tested hull form, loading conditions and forcing cases

The hull used in the present study is a model of a trawler-fishing

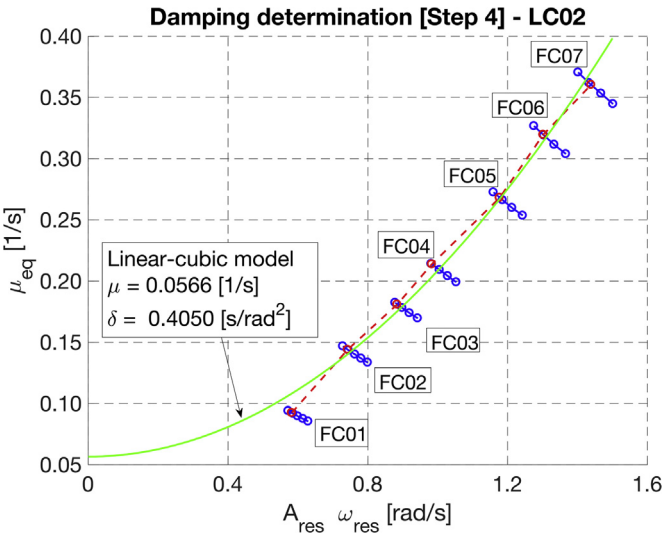

Fig. 6. Damping determination: Step 4.

vessel at scale 1:20.667. The body plan of the ship is illustrated in Fig. 7, while Fig. 8 shows a picture of the experiments. Table 1 summarizes the main particulars of the ship and Table 2 reports the details of the two considered loading conditions (LC01 and LC02). The model was tested in bare hull condition, i.e. without rudder and without bilge keels.

With reference to data reported in Table 2 (at full scale), the model displacement was determined from direct weighting. The metacentric heights (herein corresponding to *QM*) in the two loading conditions have been determined from inclining tests (see the system in Fig. 3) considering also large inclinations angles. Comparisons between $\overline{QZ}(\phi)$ curves determined from free trim hydrostatic calculations and experimentally measured ones are shown in Fig. 9 (for LC01) and Fig. 10 (for LC02). It can be seen that the agreement is very good, which provided confidence on the determined metacentric heights and it provided also confidence regarding the agreement between the reference geometry for computations and the model as actually built.

The roll natural frequency reported in Table 2 was determined from the direct analysis of roll decays (see details in the Appendix). Instead, the dry roll radius of inertia k_{xx} was not measured, but it was estimated

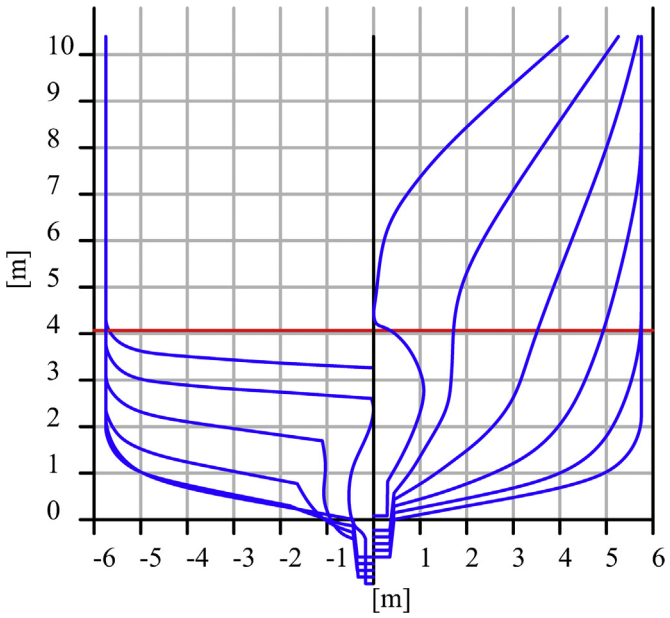

Fig. 7. Body plan of the tested hull form.

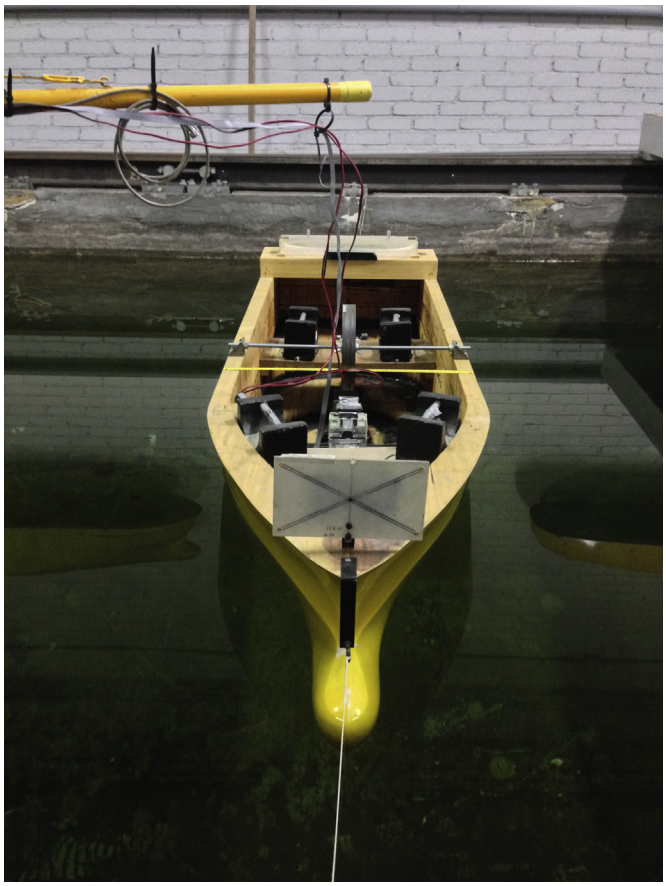

Fig. 8. Picture of the experiments.

Table 1
Main ship particulars. Model scale 1:20.667.

Length between perpendiculars, L_{pp} [m]	34.80
Length overall, *LOA* [m]	41.70
Breadth overall, B [m]	11.50
Draught, T [m]	4.07
Depth to upper deck, H [m]	11.94

indirectly from the measured roll natural frequency ω_0 and using linear seakeeping ship motion equations, considering coupled roll-sway-yaw. For this computation, hydrodynamic coefficients were determined from strip theory calculations using an in-house code (Bulian and Francescutto, 2009). The radius k_{xx} reported in Table 2 is the dry roll radius of inertia with respect to Q for the vessel comprising the moving mass placed at the centreplane. It is anticipated that, in the following analysis based on the model (7), some re-tuning of radii of inertia k_{xx} will be necessary to have a better matching between experimental and numerical roll response curves (in accordance with "Step 3" of the described procedure).

For each loading condition, different forcing cases were tested, with characteristic parameters reported in Table 3 (LC01) and Table 4 (LC02).

Table 2
Main characteristics of considered loading conditions: total mass (m_T), metacentric height (*QM*), natural roll frequency (ω_0) and estimated dry roll radius of inertia (k_{xx}). Model scale 1:20.667.

Loading Condition	m_T [t]	*QM* [m]	ω_0 [rad/s]	k_{xx} [m]	k_{xx}/B [$-$]
LC01	973	0.773	0.595	3.903	0.339
LC02	973	1.062	0.750	3.529	0.307

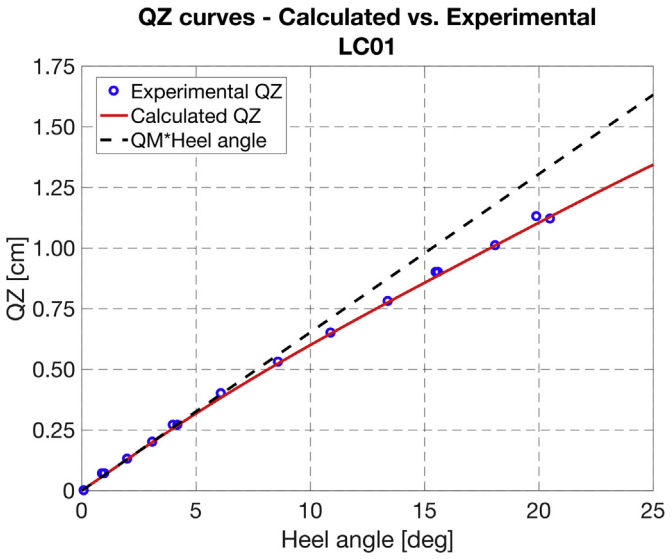

Fig. 9. Comparison between experimental and calculated QZ curve of the ship model: LC01.

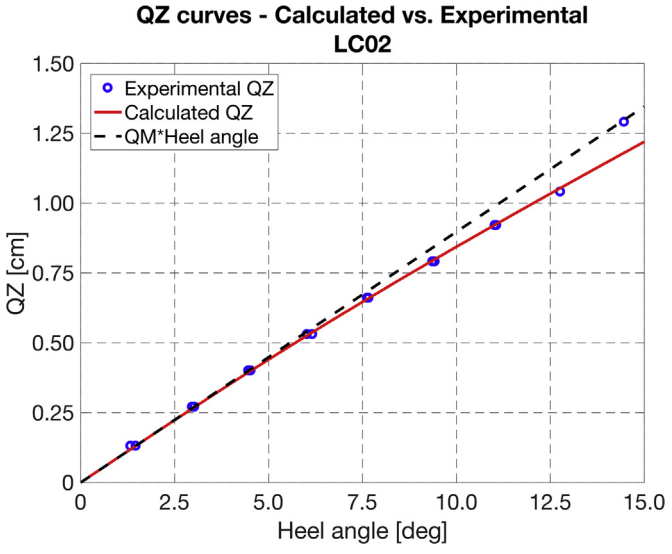

Fig. 10. Comparison between experimental and calculated QZ curve of the ship model: LC02.

Since the amplitude of moving mass motion is kept constant ($y_{m,max}$=0.09 m), changing the forcing case corresponds to changing the moving mass. In order to keep the same vertical position of the point Q from one FC to the other, the difference between the moving mass for the strongest forcing case and the one under analysis was placed near the linear rail, at the centerplane and at the same height of the linear rail. With this experimental arrangement, for each forcing case and for each loading condition, part of the mass conceptually moves from being considered as "moving mass" to being considered as part of the "ship without moving mass". However, the total mass of the model as well as the total dry roll moment of inertia considering the moving mass on the centreplane remain constant (under the approximation of point moving masses). As a result, with reference to the mathematical model (5), the considered experimental arrangement is such that the following terms can be considered, at least with good approximation, as constants:

$$\begin{cases} m_s + m_m = m_T = constant \\ I_{G_s,s,xx} + m_s\delta^2_{G_s,z} + m_m\delta^2_{m,z} = I_{O,T,xx} = I_{Q,T,xx} + (m_s + m_m)\delta^2_{Q,z} = constant \end{cases} \tag{13}$$

The values of α_{FC} for each forcing condition, as reported in Table 3 (LC01) and Table 4 (LC02), have been determined as solutions of the following equilibrium equation:

$$(m_s + m_m)g\overline{QZ}(\alpha_{FC}) = A_{FC}\cos(\alpha_{FC}) \tag{14}$$

using $\overline{QZ}(\phi)$ from hydrostatic calculations.

Table 3
Forcing cases for LC01.

	LC01				
Parameter	FC01	FC02	FC03	FC04	FC05
m_m [kg]	0.388	0.774	1.162	1.567	2.323
A_{FC} [Nm]	0.343	0.683	1.026	1.384	2.051
α_{FC} [deg]	0.49	0.97	1.46	1.97	2.93

Table 4
Forcing cases for LC02.

	LC02						
Parameter	FC01	FC02	FC03	FC04	FC05	FC06	FC07
m_m [kg]	0.539	1.076	1.618	2.133	3.228	4.283	5.378
A_{FC} [Nm]	0.476	0.950	1.429	1.883	2.850	3.781	4.748
α_{FC} [deg]	0.49	0.98	1.47	1.95	2.95	3.93	4.97

3.2. Excited roll tests results

The experiments were carried out at the ETSIN Towing Tank, having dimensions of 100 m in length, 3.8 m in breath and 2.2 m in depth. The ship model was placed transversally at mid-length of the tank to minimize the effect of reflected waves and to maximise the usable test time before coming back of waves reflected from tank ends. In the following, first, measured roll response curves for the two loading conditions and the various forcing cases are reported. Afterwards, information from a repeatability analysis is reported as well.

3.2.1. Roll response curves

The roll-response curves, as a function of the excitation frequency, for each loading condition and for each forcing case are shown in Fig. 11 (LC01) and Fig. 12 (LC02). The reported reference amplitudes for each test represent the average rolling amplitudes within the analysis time window based on the analysis of maxima and minima of roll. Considering that experimental roll motion, despite the nonlinearities of the system, was almost sinusoidal in all relevant steady state conditions, the rolling amplitude based on the analysis of extremes is well representative of the actual magnitude of motion. In addition, an indication of the uncertainty level due to variability of rolling amplitude is also presented through bars corresponding to the maximum and minimum rolling amplitudes in the analysed time window. The analysis time window for each test was decided by trying to reduce the effect of the initial transient and by avoiding the analysis of portions of recorded time history which might have been affected by reflected waves from the tank ends (wavemaker side and beach side). Nevertheless, in some cases, oscillations of roll envelope were still present due to transient effects, and the magnitude of such oscillations is represented by the variability range shown in the figures.

From Figs. 11 and 12, in both loading conditions a clearly noticeable secondary lower frequency peak can be observed, which becomes more evident as the roll angles increase. This secondary peak was an unexpected result, which the present modelling, as it will be shown later, cannot capture. The actual source of this secondary peak could not be fully clarified. However, it seems a parasitic peak which appears because, when the ship is excited to roll at large angles, pitch and heave motions are also excited due to nonlinear coupling, part of which can be explained

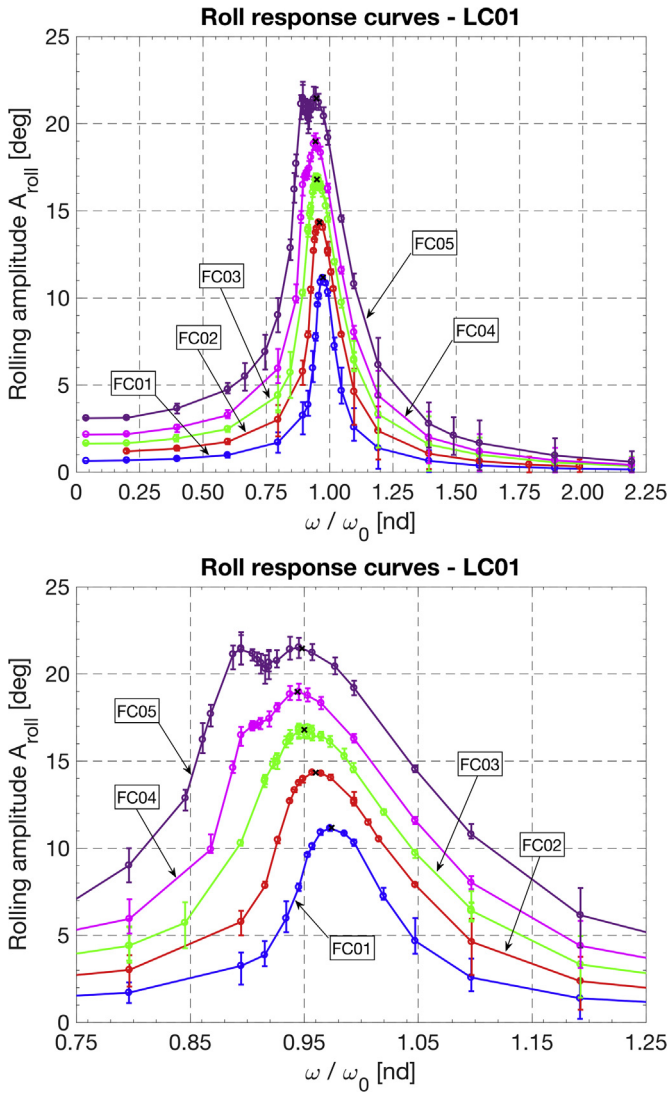

Fig. 11. Experimental roll response curves for LC01: full results (top) and zoom close to the peak region (bottom). Black cross markers represent smoothed peaks which were used for the analysis.

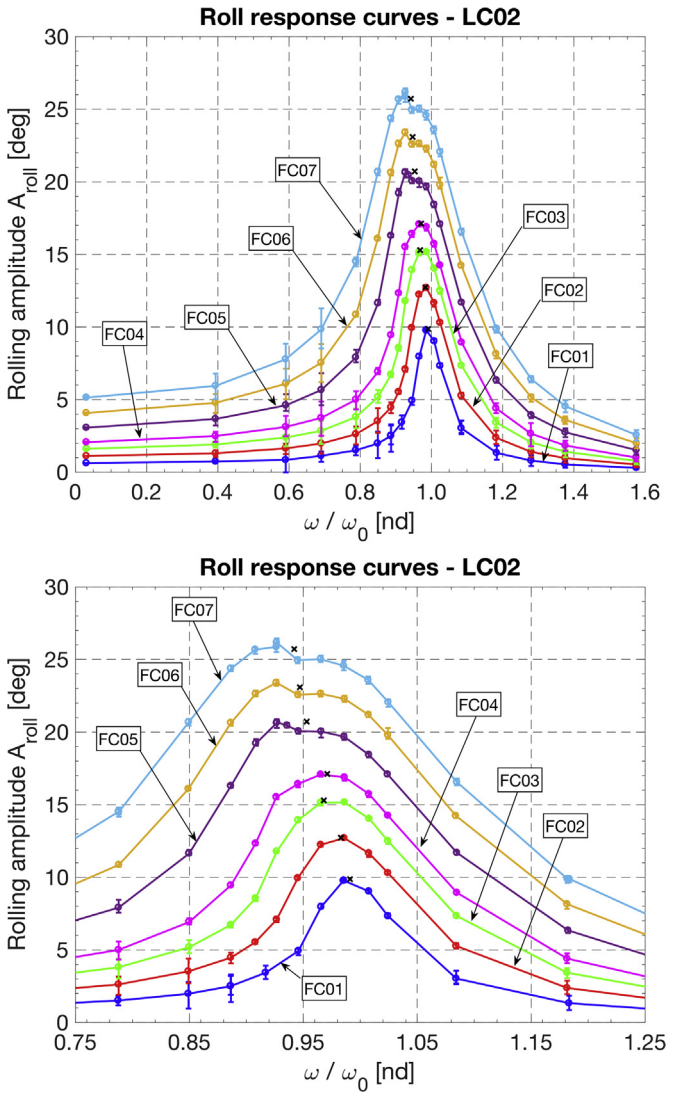

Fig. 12. Experimental roll response curves for LC02: full results (top) and zoom close to the peak region (bottom). Black cross markers represent smoothed peaks which were used for the analysis.

from buoyancy effects. Due to the symmetry of the system, heave and pitch are excited with a frequency which is double the roll oscillation frequency. The excitation of longitudinal motions generates waves propagating in longitudinal direction with respect to the vessel and reflecting on the tank walls. These waves, in some conditions, tend to generate a wave field around the model which eventually affects the roll motion of the ship. During the tests, this effect could be clearly noticed visually for LC01, while this effect was less noticeable from visual observations for LC02. This difference in the magnitude of the visually observed wave reflection phenomenon between the two loading conditions appears to be in line with the relative magnitude of the secondary peak, which is larger for LC01 compared to LC02.

In order to address the presence of this secondary peak, a smoothing polynomial was used to represent the peak region of each roll response curves, and reference peak amplitudes A_{res} and corresponding frequencies ω_{res} were determined from the polynomial smoothing curve. The corresponding points are reported in Figs. 11 and 12 as black cross markers. The numerical values for ω_{res}/ω_0 and for A_{res} as obtained from the experiments for the two loading conditions are summarised in Table 5. It is important to highlight that the applied smoothing procedure may influence the peak points used for the determination of roll damping. For instance, in LC02 and FC03 (see Fig. 12), the actual peak seems to be at a higher frequency compared to that determined by the polynomial smoothing. However, this effect appears to have a limited importance considering the various assumptions of the overall damping assessment procedure.

3.2.2. *Repeatability analysis*

In order to assess the precision level of roll measurements, an analysis of the repeatability of the tests was carried out. The level of repeatability was assessed by repeating three times different run conditions, considering the resonance frequency region as well as the regions of low and high frequencies. It is noted that repeated tests are directly represented in Figs. 11 and 12. However, since the repeatability is very high, as described in the following, the different points basically overlap in the graphs.

An example of the roll time histories of three repeated tests is shown in Fig. 13, while Table 6 and Table 7 summarise the experimentally obtained mean amplitudes for each repeated test condition. Moreover, the relative percentage difference with respect to the first run of each test condition is also reported. From the reported results, it can be concluded that the repeatability level, hence the precision of the tests is very good. In fact, the relative difference of amplitudes is typically below 1.5% with some cases presenting higher relative differences which, however, are

Table 5
Peak amplitudes and corresponding normalised frequencies for each forcing case.

Forcing case	LC01		LC02	
	ω_{res}/ω_0 [−]	A_{res} [deg]	ω_{res}/ω_0 [−]	A_{res} [deg]
FC01	0.974	11.18	0.991	9.87
FC02	0.960	14.34	0.983	12.73
FC03	0.950	16.80	0.968	15.30
FC04	0.944	18.98	0.971	17.12
FC05	0.948	21.46	0.953	20.72
FC06	–	–	0.947	23.09
FC07	–	–	0.942	25.72

always below 2.5% for the considered conditions.

It is also important to highlight that there is high repeatability also for forcing frequencies that correspond to the previously discussed secondary parasitic peak. For instance, for LC01 in FC04, the relative difference at $0.90\omega/\omega_0$, which corresponds to the secondary peak, is below 1.0% (see Table 6). This provides confidence with respect to the fact that the observed secondary peak is a repeatable physical phenomenon.

3.3. Determination of roll damping coefficients

Starting from experimental data as reported in Table 5, roll damping coefficients have been determined for the two loading conditions following the methodology described in section 2.3. It is noted, in particular, that "Step 3" (i.e. the iterative tuning of the dry inertia) was also carried out. In both cases a linear-cubic damping model was considered as reference model, as the fitting of the other models (linear-quadratic or linear-quadratic-cubic) led to negative damping coefficients and/or to overall negative linear equivalent roll damping coefficient at small rolling amplitudes.

The reason why it was necessary to re-tune the dry roll radii of inertia is that, using nominal values based on the global dry radii of inertia estimated in Table 2, the simulated roll-response curves showed a shifting of the peak frequencies compared to the experimental data. This shift was systematic, and simulated roll peak frequencies were lower than the ones observed in the experiments, for all forcing cases, as depicted in Fig. 14 and Fig. 15. The actual reasons for the observed shifts have not been fully clarified. However, the shifting may be, at least partially, a consequence of the fact that model (5), and, as a consequence, model (7), account only for roll and sway coupling, without actually considering the coupling with yaw. Lack of coupling with yaw is missing both from a hydrodynamic perspective as well as from the point of view of rigid body dynamics. Instead, the estimated global radii of inertia reported in Table 2 implicitly accounts also for the linear coupling with yaw. Moreover, calculations of hydrodynamic coefficients have been based on strip-theory and they do not account, therefore, for three-dimensional effects. Three-dimensional effects might be non-negligible for the considered vessel, which has a relatively small L/B ratio. Because of the various simplifications and assumptions in the derivation of the model (7), it may therefore be expected that some physical phenomena are not properly accounted for. Since the most noticeable effect has been observed to be the underestimation of the resonance frequencies, this has therefore been addressed by a reduction of the dry roll radii of inertia used in the mathematical model, which proved to be an effective means to obtain a better matching.

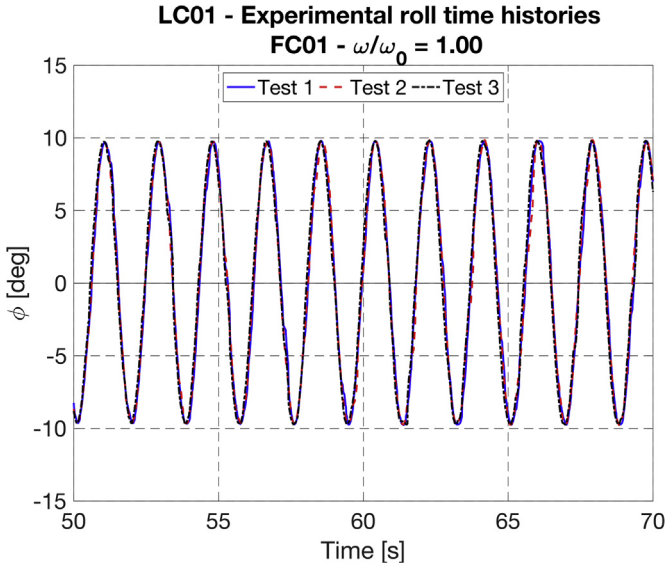

Fig. 13. Example of repeatability assessment for LC01.

Table 6
Repeatability analysis for LC01.

FC03					
ω/ω_0 [nd]	A_{roll} [deg]	Rel. Diff [%]	ω/ω_0 [nd]	A_{roll} [deg]	Rel. Diff [%]
0.80	4.40	–	0.94	16.77	–
	4.40	0.00		16.76	−0.06
	4.42	0.46		16.91	0.84
0.93	14.95	–	0.96	16.42	–
	15.20	1.67		16.79	2.25
	14.80	−1.00		16.48	0.37
FC03			FC04		
1.10	6.49	–	0.90	17.05	–
	6.41	1.23		16.90	−0.88
	6.41	1.23		16.97	−0.47

Table 8 reports the roll damping coefficient as obtained from the fitting of model (7) on the experimental roll response peaks using a linear equivalent roll damping model after tuning of the dry inertia. The table also reports initial guess values of linear equivalent roll damping coefficient as obtained from (10). It can be noticed that initial guess values are systematically smaller that the values of μ_{eq} which are eventually obtained from the proposed procedure. Table 9 then shows the values of roll damping coefficients μ and δ as obtained from fitting (11), fixing β to zero, starting from μ_{eq} in Table 8.

Fig. 16 and Fig. 17 provide a graphical representation of the fitting of damping model for the determination of damping coefficients for LC01 and LC02, respectively. In addition to the fitting based on the reference linear-cubic model, the figures also report the results of fitting of the linear-quadratic-cubic roll damping model.

From the results in Fig. 16 it can be noted that for LC01 the linear-cubic model is able to accurately fit the μ_{eq} data, with a relatively larger difference for FC04 which, however, seems to be outside the general trend from the other forcing cases. It can also be noticed that data

Table 7
Repeatability analysis for LC02.

FC01			FC07		
ω/ω_0 [nd]	A_{roll} [deg]	Rel. Diff [%]	ω/ω_0 [nd]	A_{roll} [deg]	Rel. Diff [%]
0.90	9.77	–	0.80	14.52	–
	9.79	0.20		14.52	0.00
	9.77	0.00		14.51	−0.07
1.00	2.53	–	0.94	25.86	–
	2.50	−1.19		26.17	1.20
	2.51	−0.79		26.17	1.20
1.10	3.03	–	1.20	9.89	–
	3.03	0.00		9.89	0.00
	3.03	0.00		9.89	0.00

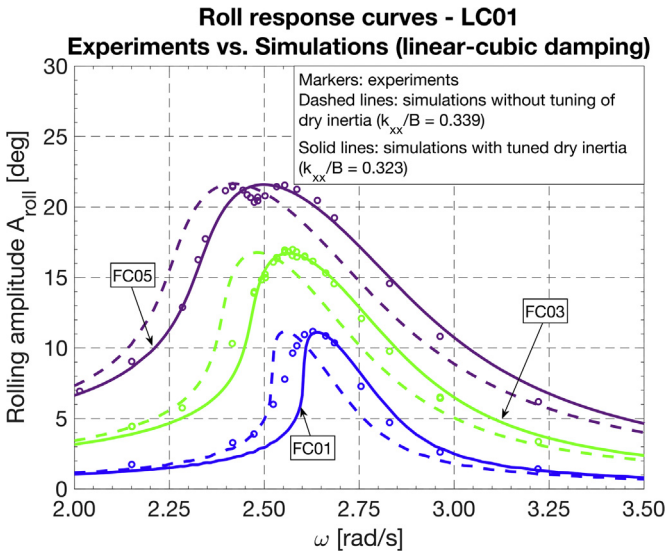

Fig. 14. Roll response curves for LC01. Effect of tuning of dry roll radius of inertia.

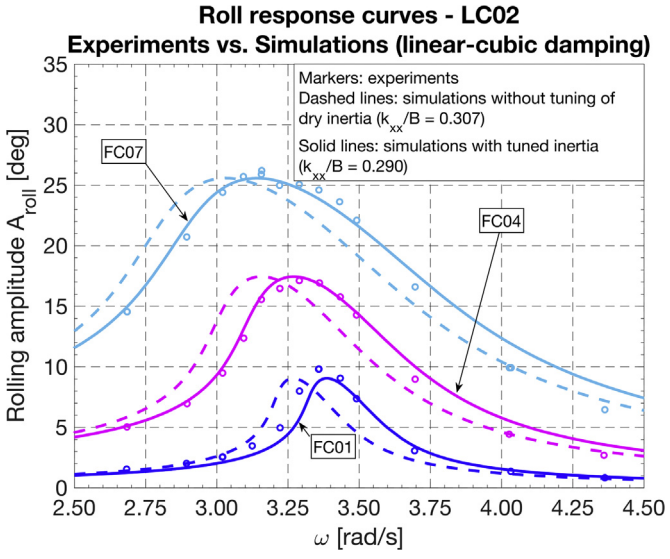

Fig. 15. Roll response curves for LC02. Effect of tuning of dry roll radius of inertia.

Table 8
Linear equivalent roll damping coefficient for each loading condition and forcing case, using tuned dry roll inertia. Values in parentheses preceded by "i.g." (initial guess) are initial guess damping values as obtained from eq. (10).

	μ_{eq} [1/s]	
Forcing Case	LC01	LC02
FC01	0.0632 (i.g. 0.0603)	0.0924 (i.g. 0.0854)
FC02	0.0994 (i.g. 0.0914)	0.1439 (i.g. 0.1334)
FC03	0.1282 (i.g. 0.1232)	0.1809 (i.g. 0.1696)
FC04	0.1537 (i.g. 0.1479)	0.2137 (i.g. 0.1991)
FC05	0.2022 (i.g. 0.1930)	0.2681 (i.g. 0.2535)
FC06	–	0.3195 (i.g. 0.3038)
FC07	–	0.3603 (i.g. 0.3446)

are well represented, in principle, also by the linear-quadratic-cubic model which, however, is associated to a negative quadratic damping coefficient. It can also be noticed that, while both the linear-cubic and

Table 9
Roll damping coefficients for each loading condition, using tuned dry roll inertia.

Damping coefficients	LC01	LC02
μ [1/s]	0.0065	0.0566
β [1/rad]	0.0000 (fixed)	0.0000 (fixed)
δ [s/rad^2]	0.5702	0.4050

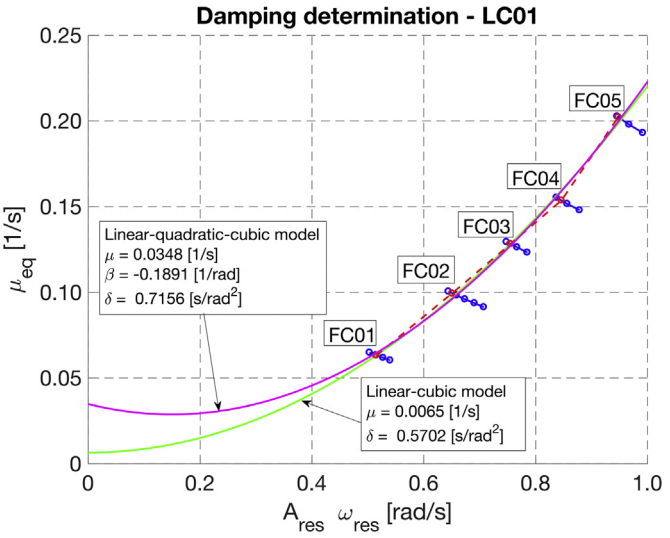

Fig. 16. Damping determination for LC01.

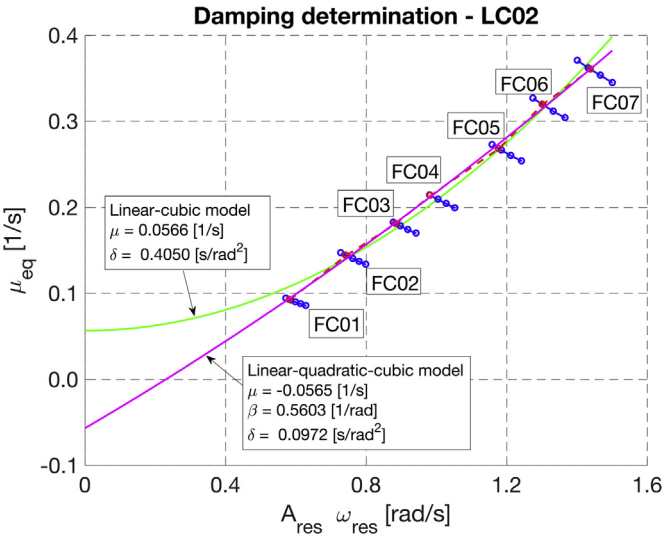

Fig. 17. Damping determination for LC02.

linear-quadratic-cubic models, thanks to the fitting constraint, show similar μ_{eq} within the experimentally tested range, they show significant differences in the region of small rolling amplitudes. This is due to the lack of experimental data from excited roll tests in the region of low amplitude rolling.

Results in Fig. 17 for LC02 show that the linear-cubic model can provide a reasonable fit of the experimental data, although the fitting is worse compared to LC01. In particular, the linear-cubic model shows difficulties in fitting experimental damping at the smallest forcing, and the curvature which is implicit in the assumed linear-cubic model does not seems to be present in the experimental data. For LC02, the flexibility of the full linear-quadratic-cubic model provides a better fitting of data in the range of tested rolling amplitudes compared to the linear-cubic

model. However, the linear-quadratic-cubic model leads to a negative linear damping coefficient and it therefore provides overall negative linear equivalent roll damping coefficients for the range of small rolling amplitudes, which is clearly unphysical. Also in this case the differences between the two models are relatively small in the range of tested rolling amplitudes, thanks to the constraint induced by the fitting of the data. However, the two modelling show significant differences in the region of small rolling amplitudes and this, again, is due to the lack of experimental data from excited roll tests in the region of small amplitude rolling.

3.4. *Validation of the mathematical model*

This section provides a validation of the mathematical model (7). In fact, once roll damping coefficients have been determined according to the described procedure, the mathematical model (7) can be used for simulating roll motion in the experimental forcing cases. Comparison of simulation results with experiments, both in terms of roll response curves and in terms of roll time histories, can then be used to validate the used mathematical model.

Fig. 18 (for LC01) and Fig. 19 (for LC02), show comparisons of experimental roll response curves and numerical simulations based on the mathematical model (7), as a function of the excitation frequency (ω). For the simulations, the damping coefficients specified in Table 9 have been used for the two considered loading conditions. As previously reported, linear hydrodynamic coefficients, for each excitation frequency, have been determined from linear strip-theory calculations. However, in order to match the experimental roll response curves, it was necessary to retune the dry roll radii of inertia of the model, as specified in the previous section.

From the results in Figs. 18 and 19, it can be observed that the matching between experiments and simulations is best around the peak of the response curves, and it worsens outside the resonance zone. One possible reason for this discrepancy may be that the mathematical model, due to the introduced simplifications, misses some relevant excitation forces and moments and/or some coupling effect among different motions.

Finally, for both loading conditions, the simulated and the experimental roll response curves for the milder forcing case (FC01) present a worse matching compared to larger forcing conditions. Part of this lack of matching can be associated with the fact that the linear-cubic roll damping model does not accurately represent roll dissipation at small rolling amplitudes, which are outside the fitting region (see Figs. 16 and 17).

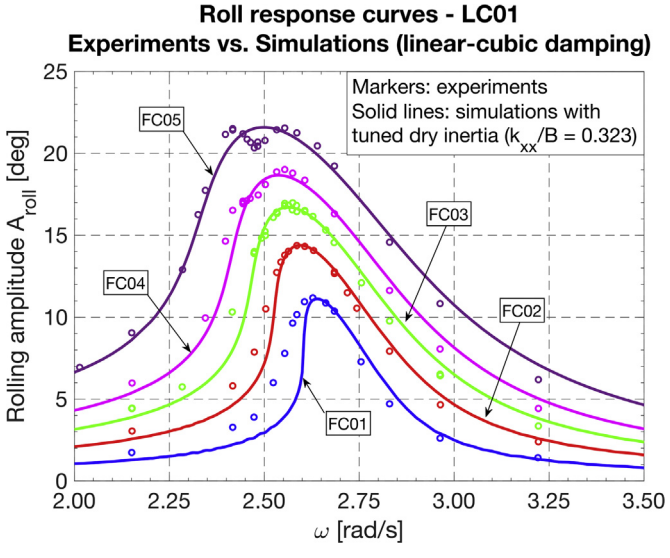

Fig. 18. Roll response curves for LC01. Comparison between experimental data and simulations (linear-cubic damping model, tuned dry roll inertia).

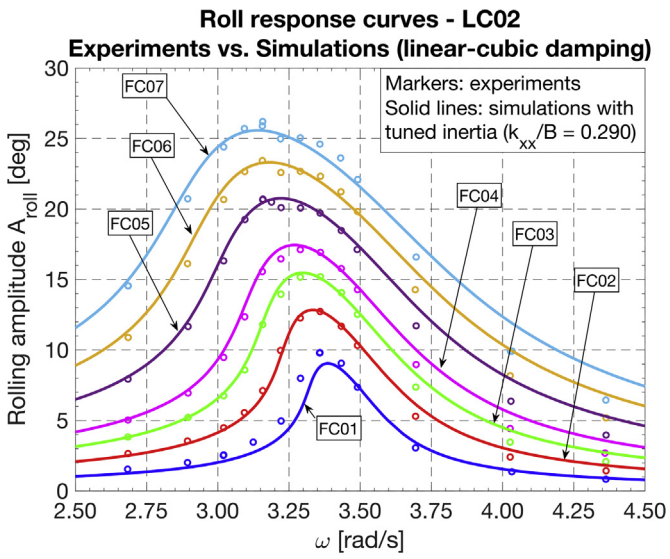

Fig. 19. Roll response curves for LC02. Comparison between experimental data and simulations (linear-cubic damping model, tuned dry roll inertia).

Notwithstanding the previously discussed differences between simulations and experiments in terms of rolling amplitudes, the mathematical model (7), after the tuning of dry roll radii of inertia, can reproduce the behaviour of experimental roll time histories, both in the transient region as well as at steady state, with a very good accuracy. Fig. 20 (LC01) and Fig. 21 (LC02) show two sets of example comparisons of simulated and experimentally measured roll time histories for forcing frequencies around the roll natural frequency. As it can be seen from the figures, although some differences can be observed in the amplitude of motion, the mathematical model (7), despite its simplicity, very well captures the general behaviour of measured roll for the whole recording period, i.e. both in the very initial transient as well as, later, in the steady state regime. It is also to be highlighted that the capability of model (7) to reproduce the measured roll behaviour is not limited to frequencies which are (relatively) close to the roll natural resonance. This can be seen in Fig. 22, which compares experimental and simulated roll time histories in a condition with high frequency forcing for LC01. From the time

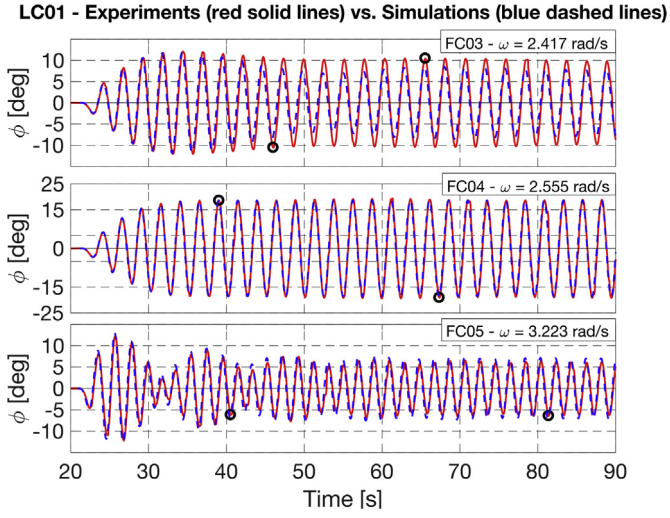

Fig. 20. LC01. Comparison between experimentally measured and numerically simulated roll motion. Different forcing cases with frequencies close to roll natural frequency. Black-circles define the time windows used for the analysis of rolling amplitude.

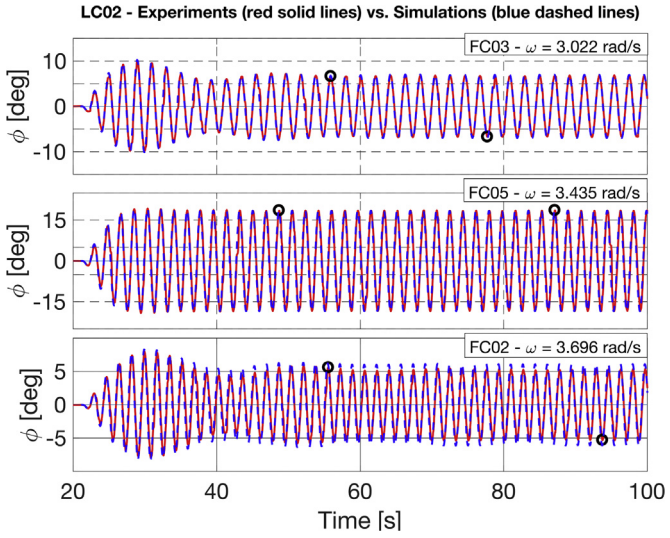

Fig. 21. LC02. Comparison between experimentally measured and numerically simulated roll motion. Different forcing cases with frequencies close to roll natural frequency. Black-circles define the time windows used for the analysis of rolling amplitude.

histories in the figure it can be noted that, although the simulated roll motion tends to overestimate the experimental one, simulations are capable of very well reproducing the quite complex transient condition.

3.5. Roll damping estimation: comparison between excited tests and decay tests

As previously mentioned, and as described by Handschel et al. (2015) and by Wassermann et al. (2016), different experimental techniques can be used to estimate roll damping, and each technique involves a different hydrodynamic scenario. It is therefore possible that damping coefficients obtained from different types of tests may differ. Handschel et al. (2015) and Wassermann et al. (2016) compared nonlinear roll damping obtained from harmonically excited tests using contra rotating masses with damping obtained from roll decays, with and without forward speed, for the post panamax containership DTC (el Moctar et al., 2012). Their results did not indicate significant differences between damping

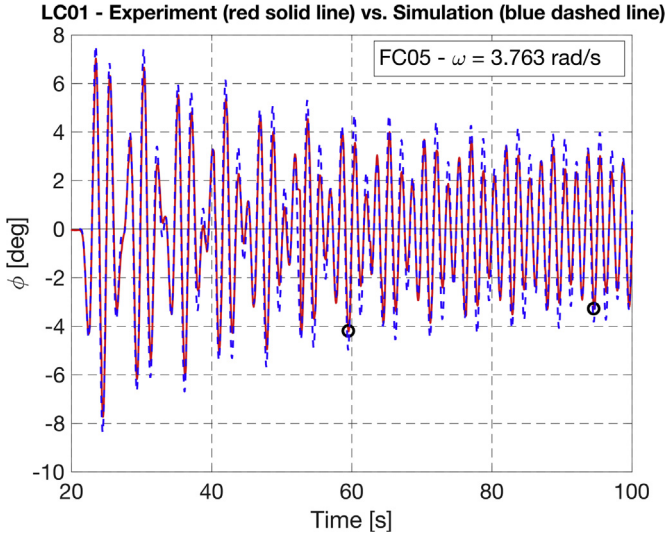

Fig. 22. LC01. Comparison between experimentally measured and numerically simulated roll motion. Example case with high frequency forcing. Black-circles define the time window used for the analysis of rolling amplitude.

estimations from the two experimental approaches. However, to the best of the authors' knowledge, no extensive work has been presented in literature in this respect. At the same time, roll damping plays a fundamental role in the prediction of ship roll motion and this aspect may become particularly critical for ship safety assessment and when applying, e.g., international regulations requiring roll damping as a parameter (e.g. IMO, 2006, 2016). It is therefore important to further assess whether different experimental techniques may lead to differences in estimated roll damping, which may potentially influence to a non-negligible extent ship motions predictions and/or regulatory assessments.

To this end, experimental roll decay tests have been carried out for the two considered loading conditions, and damping estimated from the analysis of roll decays is compared in this section with damping obtained from the proposed procedure based on internally excited tests. The analysis of the decay tests has been carried out following Bulian et al. (2009), as described in the Appendix. The applied procedure considers nonlinearities in the restoring and in the damping terms, and it is based on the analysis of roll decrements. Multiple roll decay tests have been executed, and data from roll decrement analysis have been combined. Results from the analysis are shown in Fig. 23 (for LC01) and Fig. 24 (LC02). Each figure shows the amplitude dependent linear equivalent roll damping and the amplitude dependent equivalent roll frequency. Together with raw data, solid curves are also reported. In case of equivalent linear roll damping coefficient, the solid curve for each loading condition was obtained by fitting a linear-cubic roll damping model to the available data, taking into account the amplitude dependence of the roll oscillation frequency. In case of the equivalent roll natural frequency, the solid curve represents the amplitude dependent roll oscillation frequency as obtained from the calculated $\overline{QZ}(\phi)$ curve (see Bulian et al., 2009) and using, as free fitting parameter, only the roll natural frequency ω_0, as described in the Appendix. Considering the small values of dimensionless damping, which is a peculiar feature of roll motion even at large rolling amplitudes, in the analysis, the difference between the damped and undamped oscillation frequencies has been neglected.

Fig. 25 (LC01) and Fig. 26 (LC02) report a comparison of amplitude dependent μ_{eq} as obtained by linear-cubic roll damping models derived from the analyses of decay tests and of excited roll tests using the internal moving mass. The reported results indicate that, for the considered vessel, the nonlinear roll damping estimated from the two techniques show clear differences, which are larger for LC01 and smaller for LC02. However, it is important to underline that the ranges

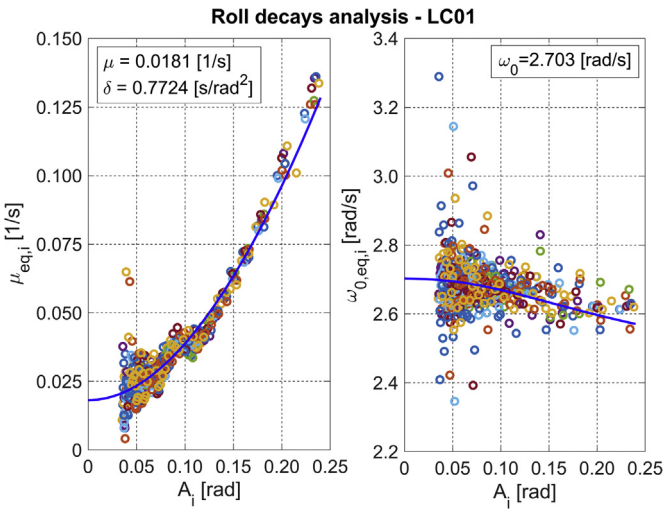

Fig. 23. Analysis of roll decay tests for LC01. Amplitude dependent linear equivalent roll damping coefficient (left) and amplitude dependent equivalent roll natural frequency (right).

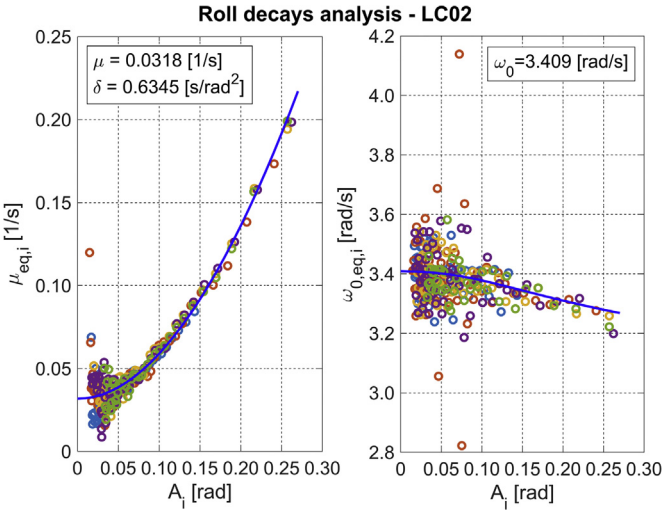

Fig. 24. Analysis of roll decay tests for LC02. Amplitude dependent linear equivalent roll damping coefficient (left) and amplitude dependent equivalent roll natural frequency (right).

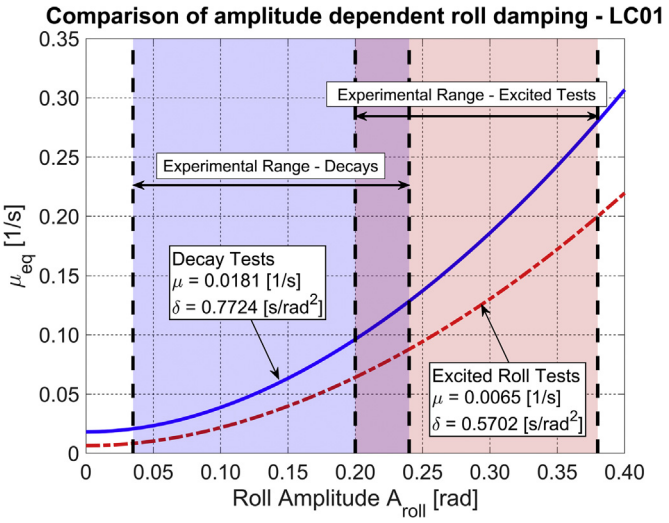

Fig. 25. LC01. Comparison of amplitude dependent linear equivalent roll damping coefficient as obtained from roll decays and from internally excited roll tests.

of rolling amplitudes on which the two techniques have based the fitting of roll damping coefficients are different, and the two ranges only partially overlap. While data from roll decays cover the range of smaller rolling amplitudes, peaks of the roll response curves from the excited roll experiments cover, instead, the range of larger rolling amplitudes. As a result, the more meaningful comparisons should be based on data contained in the overlapping range of rolling amplitudes. It is also to be noted that, due to the lack of data from excited roll tests in the region of smaller amplitudes, μ_{eq} in that region as predicted by the fitted roll damping model is strongly dependent on the assumed analytical form of nonlinear roll damping (linear-cubic in this case). In fact, very different results are obtained in that region depending on the selected form of roll damping model (see Figs. 16 and 17). Instead, damping obtained from roll decays in the region of small rolling amplitudes is constrained by actual data and not by analytical assumptions, and it therefore reflects the actual physics in

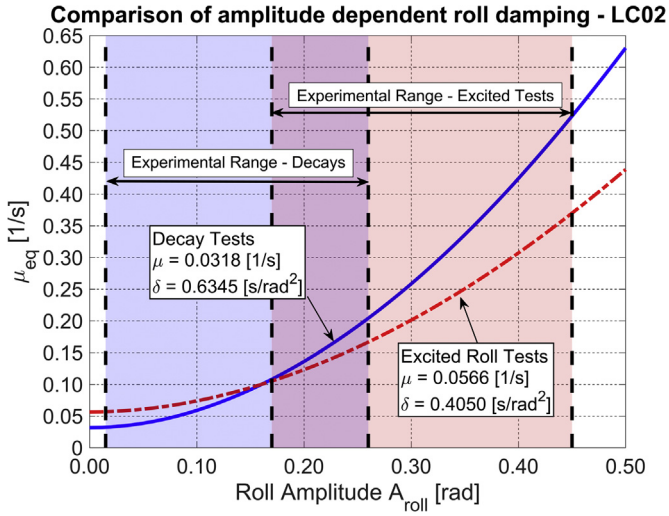

Fig. 26. LC02. Comparison of amplitude dependent linear equivalent roll damping coefficient as obtained from roll decays and from internally excited roll tests.

the corresponding experimental technique.

For the considered vessel, in the overlapping range of amplitudes, roll damping estimated from roll decays tend to be larger than that obtained from excited roll tests for both tested loading conditions. This is evident and systematic in case of LC01, whereas this tendency is smaller and limited to the range of large roll amplitudes in case of LC02. Part of the differences may be ascribed to the completely different procedures for the analysis of the experimental data, since the two experimental techniques are completely different. However, part of the discrepancy could also be associated with the different hydrodynamic scenarios in the two cases. In fact, in case of roll decays, the water is initially at rest, and roll dissipation, at least in the initial cycles, occur in a transient condition. Instead, damping obtained from internally excited roll tests is based on steady state rolling motion, where the initial transient has already completed (to a large extent), and the system is undergoing (almost) harmonic periodic motions.

From an application (design and/or regulatory) perspective, roll damping is determined (numerically or experimentally) in order to be eventually used for roll motion predictions in waves (see, e.g., Kuroda et al. (2003), Míguez González et al. (2013), Neves et al. (2003), Paroka and Umeda (2006, 2007), for the specific case of fishing vessels). Between the two considered experimental techniques, and considering the characteristics of the two hydrodynamic scenarios, it may be conjectured that the roll dissipation estimated from excited roll tests may be more appropriate for being used for prediction of roll motion in waves. However, at this moment, this remains a qualitative conjecture. Further tests should be carried out to verify whether the observed differences in roll damping estimation from the two techniques are confirmed also in other cases, since the results obtained herein for the considered fishing vessel are not in line with those obtained from Handschel et al. (2015) and Wassermann et al. (2016) for the DTC containership. In this respect, it may be possible that differences among methodologies could depend on the characteristics of the considered hull form. Moreover, in order to decide on the most appropriate technique for roll damping determination, roll experiments in waves should be used as a reference. Numerical roll motion predictions based on roll damping estimated by different approaches should then be compared to experimental data, in order to conclude on the roll damping values providing, eventually, the best prediction capabilities.

4. Conclusions

The paper presented a methodology for the determination of roll damping coefficients starting from excited roll tests in calm water. The proposed excited roll tests are based on the generation of roll excitation through the sinusoidal transversal movement of a mass inside the ship model. In the considered tests, the model is free (or at most softly restrained) in calm water. A 1-DOF mathematical model for roll motion, which embeds coupling with sway, has been developed to describe the dynamics of the system and to be used as a tool for the determination of roll damping coefficients from experimental roll response curves. A procedure for the analysis of experimental data has been described. The proposed methodology allows to obtain ship roll damping up to large rolling amplitude, which is typically difficult (or, in some cases, impossible) if more common roll decay experiments are used.

An application case study has been presented, and described in detail, where the model of a trawler fishing vessel, in two different loading conditions, was experimentally tested through the proposed technique. Roll damping was determined according to the procedure proposed in the paper. In addition, roll decay tests were also executed. Roll damping coefficients were determined from both approaches and compared.

The case study indicated that, overall, the proposed procedure can be suitable for the determination of roll damping coefficients. The proposed mathematical model, after the fitting of nonlinear roll damping, can satisfactorily represent the experimental data. To obtain a good matching of experimental and measured roll response curves, some tuning of dry roll inertia was necessary. This may be a consequence of the fact that the proposed mathematical model only accounts for roll and sway, and it therefore misses the influence of the other degrees of freedom. Another reason for the need of tuning the dry roll inertia may be the fact that hydrodynamic coefficients have herein been calculated using a strip-theory approach and not a three dimensional approach. However, following the tuning of dry roll inertia, the obtained roll response curves were, overall, and especially near resonance, in line with those obtained from experiments. Moreover, a comparison of experimental and simulated roll time histories showed that, despite its relative simplicity, the proposed mathematical model is capable of very well capturing the behaviour of roll motion not only at steady state but also in the transient zone. Considering the observed good agreement between experiments and simulations, the developed mathematical model could be considered as a promising tool to determine roll damping, which is worth being further investigated.

From an experimental perspective, the roll response curves showed a secondary parasitic peak near the resonance frequency. This secondary peak appears to be the result of roll induced vertical motions (particularly pitch). Vertical motions generate waves which interact with the walls of the tank and, after reflection, create a disturbance also on roll motion. The presence of this secondary peak was addressed, in the data processing carried out in the paper, by smoothing of the roll response curve. However, carrying out the proposed type of tests in a seakeeping basin would reduce (practically avoid) this type of interference.

Roll damping estimated from the proposed approach showed evident differences with respect to roll damping estimated from roll decays. For one of the tested loading conditions (LC01), the amplitude dependent equivalent linear damping coefficient from the decay tests was larger than that obtained from the proposed technique for all roll amplitudes in the overlapping range of tested roll amplitudes. This tendency was observed also for the other loading condition (LC02), although it was less marked. The difference may be associated with the different hydrodynamic scenarios in the two cases. In fact, in case of roll decays, the water is initially at rest, and roll dissipation, at least in the initial cycles, occur in a transient condition. Instead, damping obtained from internally excited roll tests is based on steady state rolling motions, where the initial transient has already completed (to a large extent), and the system is undergoing (almost) harmonic periodic motions. Since roll damping is intended to be used for prediction of roll motion in waves, the discussion on which technique should be considered more suitable for damping determination should be based on the comparison of numerical roll motion predictions with experimental tests in waves.

In general, it appears that the proposed technique is worth being further investigated, because it shows significant flexibility and potentialities.

Acknowledgements

Part of the presented research activity was carried out during two research visits of Adriana Oliva Remolà at the Department of Engineering and Architecture (University of Trieste) with the financial support from the Consejo Social of the Universidad Politécnica de Madrid, which the authors would like to sincerely acknowledge. The authors would also like to thank Ricardo Abad Arroyo, Elkin Botia Vera, Daniel Celdrán Baudes, Juan Luis Chacón Gómez, Claudia Maria de la Cruz González, Iván González Navarro and Daniel Paredes Henche for their contributions, help and advice.

Appendix

Roll decays have been analysed using the procedure described in this appendix, referencing to Bulian et al. (2009). First, along the line of Roberts (1985), the roll decay envelope was filtered in order to reduce spurious effects due to the presence of possible bias. Then, for each half roll cycle (see Fig. A.1) the corresponding reference roll amplitude A_i and linear equivalent roll damping coefficient $\mu_{eq,i}$ are defined as follows:

$$\begin{cases} A_i = \dfrac{|C_i| + |C_{i+1}|}{2} \\ \mu_{eq}(A_i) = \mu_{eq,i} = \dfrac{1}{t_{i+1} - t_i} \ln\left(\dfrac{|C_i|}{|C_{i+1}|}\right) \end{cases} \tag{A.1}$$

The amplitude dependent roll oscillation frequency was determined from the peak time instants as follows:

$$\tilde{\omega}_{eq}(A_i) = \tilde{\omega}_{eq,i} = \frac{\pi}{t_{i+1} - t_i} \tag{A.2}$$

Since the system is lightly damped, it was finally assumed that the oscillation frequency $\tilde{\omega}_{eq}(A)$ is a good approximation of the undamped amplitude dependent roll oscillation frequency $\omega_{o,eq}(A)$, i.e.:

$$\omega_{0,eq}(A_i) = \omega_{0,eq,i} \approx \tilde{\omega}_{eq,i} \tag{A.3}$$

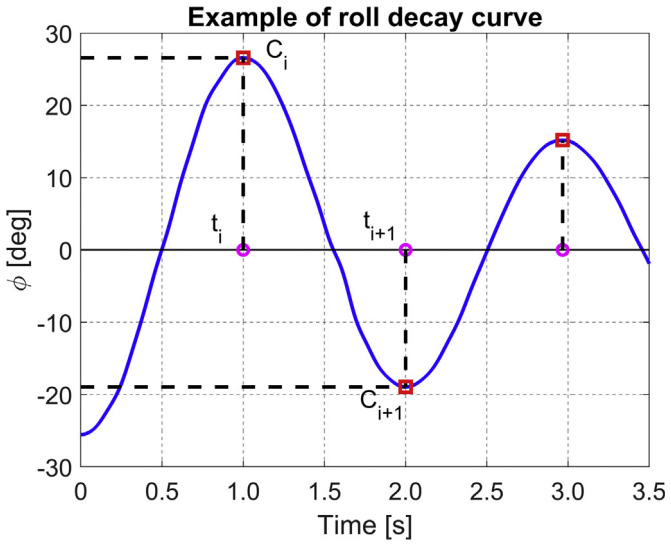

Fig. A.1. Example of roll decay curve.

In order to determine the (undamped) roll natural frequency ω_0, use was made of the link between the roll righting lever curve $\overline{GZ}(\phi)$ and the amplitude dependent (undamped) roll oscillation frequency ω_0, i.e. (Bulian et al., 2009):

$$\omega_{0,eq}^2(A) = \frac{\omega_0^2}{GM} \frac{\int_0^{2\pi} \overline{GZ}(\phi = A\cos(\alpha))\cos(\alpha)d\alpha}{\pi A} \tag{A.4}$$

Since $\overline{GZ}(\phi)$ is known from hydrostatic computations, as well as the corresponding GM, the frequency ω_0 was obtained from roll decay data as follows:

$$\omega_0 = \sqrt{\frac{1}{N}\sum_{i=1}^{N} \frac{\omega_{0,eq}^2(A_i)GM\pi A_i}{\int_0^{2\pi} \overline{GZ}(\phi = A_i\cos(\alpha))\cos(\alpha)d\alpha}} \tag{A.5}$$

In equation (A.5) the variable N represents the total number of available half cycles which were used for the analysis. It is important to underline that, in order to increase the dataset, multiple roll decays were combined together for the determination of ω_0 according to (A.5).

Furthermore, in the framework of the present tests, the $\overline{GZ}(\phi)$ curve corresponds to $\overline{QZ}(\phi)$, and GM corresponds to QM, as defined in section 2.2.2. In fact, during roll decay tests, the moving mass is positioned at its nominal position at centreplane and, therefore, the point Q coincides with the global centre of gravity of the vessel comprising the moving mass.

References

Aarsæther, K.G., Kristiansen, D., Su, B., Lugni, C., 2015. Modelling of roll damping effects for a fishing vessel with forward speed. In: Proc. ASME 2015 34th International Conference on Ocean, Offshore and Arctic Engineering (OMAE2015), May 31-June 5, St. John's, Newfoundland, Canada, Paper OMAE2015–41856.

Ali, B., Katayama, T., Ikeda, Y., 2004. Roll damping characteristics of fishing boats with and without drift motion. Int. Shipbuild. Prog. 51 (2,3), 237–250.

Bačkalov, I., Bulian, G., Cichowicz, J., Eliopoulou, E., Konovessis, D., Leguen, J.-F., Rosén, A., Themelis, N., 2016. Ship stability, dynamics and safety: status and perspectives from a review of recent STAB conferences and ISSW events. Ocean. Eng. 116, 312–349.

Bassler, C.C., 2013. Analysis and Modelling of Hydrodynamic Components for Ship Roll Motion in Heavy Weather. Ph.D. Thesis. Virginia Tech. University, 2 May.

Bertaglia, G., Scarpa, G., Serra, A., Francescutto, A., Bulian, G., 2004. Systematic experimental tests for the IMO weather criterion requirements and further development towards a probabilistic intact stability approach. In: Proc. 7th International Ship Stability Workshop (ISSW2004), 1-3 November, Shanghai, China, pp. 63–74.

Blume, P., 1979. Experimentelle Bestimmung von Koeffizienten der wirksamen Rolldämpfung und ihre Anwendung zur Abschätzung extremer Rollwinkel (Determination of Coefficients for the Effective Roll Damping by Model Tests and their Application for Estimating Large Roll Angles). Schiffstecknik Bd. 26, 3–23.

Bulian, G., 2004. Estimation of nonlinear roll decay parameters using an analytical approximate solution of the decay time history. Int. Shipbuild. Prog. 51 (1), 5–32.

Bulian, G., Francescutto, A., 2009. Experimental results and numerical simulations on strongly nonlinear rolling of multihulls in moderate beam seas. Proc. Inst. Mech. Eng. - Part M - J. Eng. Marit. Environ. 223 (2), 189–210.

Bulian, G., Francescutto, A., Fucile, F., 2009. Determination of Relevant Parameters for the Alternative Assessment of Intact Stability Weather Criterion on Experimental Basis. Report from HYDRALAB Project HYD-III-CEH-5, University of Trieste. 22 November.

Bulian, G., Souto-Iglesias, A., Delorme, I., Botia-Vera, E., 2010. Smoothed particle hydrodynamics (SPH) simulation of a tuned liquid damper (TLD) with angular motion. J. Hydraul. Res. 48 (Extra issue), 28–39.

Cardo, A., Francescutto, A., Nabergoj, R., 1982. On damping models in free and forced rolling motion. Ocean. Eng. 9 (2), 171–179.

Contento, G., Francescutto, A., Piciullo, M., 1996. On the effectiveness of constant coefficients roll motion equation. Ocean. Eng. 23 (7), 597–618.

Dalzell, J.F., 1978. A note on the form of ship roll damping. J. Ship Res. 22 (3), 178–185.

el Moctar, O., Shigunov, V., Zorn, T., 2012. Duisburg Test Case: post-panamax container ship for benchmarking. Ship Technol. Res. 59 (3), 50–64 (and see also corresponding Corrigendum in Ship Technol. Res. 60 (2), 2013, 98).

Falzarano, J., Somayajula, A., Seah, R., 2015. An overview of the prediction methods for roll damping of ships. Ocean Syst. Eng. 5 (2), 55–76.

Francescutto, A., Contento, G., Biot, M., Schiffrer, L., 1998. The effect of excitation modelling in the parameter estimation of nonlinear rolling. In: Proc. Eighth (1998) International Offshore and Polar Engineering Conference, Montréal, Canada, May 24-29, pp. 490–498.

Francescutto, A., Contento, G., 1998. The modelling of the excitation of large amplitude rolling in beam waves. In: Proc. Fourth International Ship Stability Workshop (ISSW'98), 27–28 September, St. John's, Newfoundland.

Francescutto, A., Contento, G., 1999. Bifurcations in ship rolling: experimental results and parameter identification technique. Ocean. Eng. 26 (11), 1095–1123.

Froude, W., Sir Westcott, A., Gawn, R.W.L., Duckworth, A.D., 1955. The Papers of William Froude, 1810–1879. Institution of Naval Architects.

Haddara, M.R., Bennett, P., 1989. A study of the angle dependence of roll damping moment. Ocean. Eng. 16 (4), 411–427.

Handschel, S., Köllisch, N., Abdel-Maksoud, M., 2012. Roll damping of twin-screw vessels: comparison of RANSE with established methods. In: Proc. 11th International

Conference on the Stability of Ships and Ocean Vehicles (STAB2012), 23-28 September, Athens, Greece, pp. 887–898.
Handschel, S., Abdel-Maksoud, M., 2014. Improvement of the harmonic excited roll motion technique for estimating roll damping. Ship Technol. Res. 61 (3), 116–130.
Handschel, S., Feder, D.-F., Abdel-Maksoud, M., 2015. Estimation of ship roll damping - a comparison of the decay and the harmonic excited roll motion technique for a post panamax container ship. In: Proc. 12th International Conference on the Stability of Ships and Ocean Vehicles (STAB2015), 14-19 June, Glasgow, UK, vol. 1, pp. 475–488.
Himeno, Y., 1981. Prediction of Roll Damping - State of the Art. Report No. 239, Department of Naval Architecture and Marine Engineering, College of Engineering, The University of Michigan. September.
Hua, M.T., Régnier, E., Mélice, M., Leguen, J.-F., 2011. Approximation of roll damping by a second order oscillator for experiments at different scales and numerical calculations. In: Proc. 12th International Ship Stability Workshop (ISSW2011), 12-15 June, Washington D.C., USA, pp. 317–323.
IMO, 2006. MSC.1/Circ. 1200. Interim Guidelines for Alternative Assessment of the Weather Criterion. 24 May. London, UK.
IMO, 2016. SDC4/5/1, SDC4/5/1/Add.1-Add.6. Finalization of the Second Generation Intact Stability Criteria. Report of the Correspondence Group. Part 1 to Part 7. 11 November. London, UK.
IMO, 2017. SDC4/WP.4. Finalization of the Second Generation Intact Stability Criteria. Report of the Working Group. Part 1. 16 February. London, UK.
ITTC, 2011. Numerical Estimation of Roll Damping. Recommended Procedure 7.5-02-07-04.5.
Ikeda, Y., Himeno, Y., Tanaka, N., 1978. A Prediction Method for Ship Roll Damping. Report. No. 00405 of the Department of Naval Architecture. University of Osaka Prefacture, Osaka, Japan. December.
Irkal, M.A.R., Nallayarasu, S., Bhattacharyya, S.K., 2016. CFD approach to roll damping of ship with bilge keel with experimental validation. Appl. Ocean Res. 55, 1–17.
Kawahara, Y., Maekawa, K., Ikeda, Y., 2012. A simple prediction formula of roll damping of conventional cargo ships on the basis of Ikeda's method and its limitation. J. Shipp. Ocean Eng. 2 (4), 201–210.
Kuroda, T., Matsuda, A., Hashimoto, H., Shigehiro, R., 2003. Relation between freeboard and capsizing risk for fishing vessels. In: Proc. 8th International Conference on the Stability of Ships and Ocean Vehicles (STAB2003), 15-19 September, Madrid, Spain, pp. 665–676.
Mathisen, J.B., Price, W.G., 1985. Estimation of ship roll damping coefficients. Trans. RINA 127, 295–307.
Míguez González, M., Díaz Casás, V., López Peña, F., Pérez Rojas, L., 2013. Experimental analysis of roll damping in small fishing vessels for large amplitude roll forecasting. In: Proc. 13th International Ship Stability Workshop (ISSW2013), 23-26 September, Brest, France, pp. 95–103.
Neves, M.A.S., Pérez, N.A., Rodriguez, C.A., 2003. Hull design considerations for improved stability of fishing vessels in waves. In: Proc. 8th International Conference on the Stability of Ships and Ocean Vehicles (STAB2003), 15-19 September 2003, Madrid, Spain, pp. 291–304.
Ommani, B., Kristiansen, T., Firoozkoohi, R., 2015. Nonlinear roll damping, a numerical parameter study. In: Proc. of the Twenty-fifth International Ocean and Polar Engineering Conference (ISOPE2015). International Society of Offshore and Polar Engineers. Paper ISOPE-I-15–677.
Optitrack, 2017. Optitrack Flex 3. http://optitrack.com/products/flex-3/. (Accessed 23 February 2018).
Park, J., Sung, H.G., Ahmad, F., So, S.H., Syngellakis, S., Jung, K.H., Jang, T.S., 2017. A numerical identification of excitation force and nonlinear restoring characteristics of ship roll motion. J. Mar. Sci. Technol. 25 (4), 475–481.
Paroka, D., Umeda, N., 2006. Prediction of capsizing probability for a ship with trapped water on deck. J. Mar. Sci. Technol. 11 (4), 237–244.
Paroka, D., Umeda, N., 2007. Effect of freeboard and metacentric height on capsizing probability of purse seiners in irregular beam seas. J. Mar. Sci. Technol. 12 (3), 150–159.
Peters, W., Belenky, V., Bassler, C., Spyrou, K., Umeda, N., Bulian, G., Altmayer, B., 2012. The Second Generation Intact Stability Criteria: an overview of development. Trans. Soc. Nav. Archit. Mar. Eng. (SNAME) 119 (2011), 225–264.
Roberts, J., 1985. Estimation of nonlinear ship roll damping from free-decay data. J. Ship Res. 29 (2), 127–138.
Spouge, J.R., Ireland, M., Collins, J.P., 1986. Large amplitude rolling experiment techniques. In: Proc. Third International Conference on Stability of Ships and Ocean Vehicles (STAB'86), 22-26 September, Gdansk, Poland, vol. 2, pp. 95–102.
Spyrou, K.J., Thompson, J.M.T., 2000. Damping coefficients for extreme rolling and capsize: an analytical approach. J. Ship Res. 44 (1), 1–13.
Wassermann, S., Feder, D.-F., Abdel-Maksoud, M., 2016. Estimation of ship roll damping - A comparison of the decay and the harmonic excited roll motion technique for a post panamax container ship. Ocean. Eng. 120, 371–382.